Title (12 words; 93 characters with spaces)

Bone marrow adipocytes drive the development of tissue invasive Ly6C^{high} monocytes during obesity

Running Title: Bone marrow fat linked to Ly6C^{high} monocytes in obesity

Parastoo Boroumand[1,2], David Prescott[3,4], Michael Wong[1], Jeff Shen[1], Ivan Tattoli[4], Yuhuan Zhou[1], Nancy Shi[1], Lucie Y Zhu[1], Zhi Liu[1], Angela Li[3], Tapas Mukherjee[3], Philip J. Bilan[1], Dana J. Philpott[3], Stephen E. Girardin[3,4], Amira Klip[1,2*].

[1]Cell Biology Program, The Hospital for Sick Children, Toronto, Ontario, M5G 0A4; Canada;

[2]Department of Biochemistry, University of Toronto, Toronto, Ontario, M5S 1A8; Canada;

[3]Department of Immunology, University of Toronto, Toronto, Ontario, M5S 1A8; Canada;

[4]Department of Laboratory Medicine and Pathophysiology, University of Toronto, Toronto, Ontario, M5S 1A8; Canada

*Corresponding Author:

Amira Klip, Ph.D.

Cell Biology Program

Hospital for Sick Children

Toronto, Ontario M5G 0A4, Canada

Phone: 416-813-6392

E-mail: amira@sickkids.ca

Summary (150 Words, 150):

During obesity and high fat-diet (HFD) feeding in mice, sustained low-grade inflammation includes not only increased pro-inflammatory macrophages in the expanding adipose tissue, but also bone marrow (BM) production of invasive Ly6C^{high} monocytes. As BM adiposity also accrues with HFD, we explored the relationship between the gains in BM white adipocytes and invasive Ly6C^{high} monocytes *in vivo* and through *ex vivo* paradigms. We find a temporal and causal link between BM adipocyte whitening and the Ly6C^{high} monocyte surge, preceding the adipose tissue macrophage rise during HFD. Phenocopying this, *ex vivo* treatment of BM cells with conditioned media from BM adipocytes or from *bona fide* white adipocytes favoured Ly6C^{high} monocyte preponderance. Notably, Ly6C^{high} skewing was preceded by monocyte metabolic reprogramming towards glycolysis, reduced oxidative potential and increased mitochondrial fission. In sum, short-term HFD changes BM cellularity, resulting in local adipocyte whitening driving a gradual increase and activation of invasive Ly6C^{high} monocytes.

Keywords:

Obesity; Immunometabolism, Bone marrow monocytes, Bone marrow adipocytes, Tissue invasive monocytes, Ly6C^{high} monocytes, Glycolytic shift.

40 **Introduction:**

41 A continuum of chronic obesity leading to metabolic disorders such as insulin resistance and
42 eventually type 2 diabetes is of paramount concern worldwide (Centers for Disease Control and Prevention,
43 2017; Hamann, 2017; WHO, 2016). An important contributor to the development and exacerbation of
44 insulin resistance is a gain in macrophages in adipose tissue (AT) (Liu et al., 2019; Weisberg et al., 2003),
45 muscle (Fink et al., 2014; Garvey et al., 2008) and liver (Lanthier et al., 2010) as well as their enhanced
46 pro-inflammatory (Lumeng et al., 2007, 2008; De Souza et al., 2005) and glycolytic skewing (Sharma et
47 al., 2020). This low-grade inflammation is partly explained by circulating monocyte infiltration into tissues
48 where they differentiate to pro-inflammatory macrophages (Kohyama et al., 2016).

49 Ly6C^{high} monocytes in mice, and classical CD14^{++} CD16^{-} monocytes in humans, constitute the
50 predominant tissue-infiltrating monocyte subset during chronic inflammation. These tissue-invasive
51 monocytes are classified by high surface abundance of the Ly6C protein, the chemokine receptor CCR2
52 and the adhesion molecule L-selectin, all of which allow for monocyte extravasation from the BM and
53 infiltration into the tissues (Auffray et al., 2007; Boniakowski et al., 2018; Fink et al., 2014; Geissmann et
54 al., 2003; Weisberg et al., 2006). With obesity, the development of Ly6C^{high} monocytes along with their
55 precursor cells in the BM is boosted (Griffin et al., 2018; Manicone et al., 2016; Singer et al., 2014) leading
56 to a rise in available circulating Ly6C^{high} monocytes for tissue-infiltration (Friedrich et al., 2019; Singer et
57 al., 2014).

58 Various obesity-driven factors amalgamate for greater Ly6C^{high} monocyte infiltration into the AT
59 including (a) increased AT-dependent chemoattraction (Kamei et al., 2006; Nagareddy et al., 2014; Nov et
60 al., 2013; Renovato-Martins et al., 2017) and (b) enhanced BM myelopoiesis (Griffin et al., 2018; Manicone
61 et al., 2016; Singer et al., 2014). However, it is not clear whether the obesity-induced BM myelopoiesis
62 occurs prior to, concurrently, or after the elevation of AT macrophages. Since the BM is a highly-
63 vascularized tissue, home to hematopoietic and mesenchymal lineages, and is dynamically reactive to
64 environmental changes, we reasoned it might be an early responder to HFD-induced obesity, producing
65 increased Ly6C^{high} monocytes prior to their accumulation in the AT. Further, since BM-resident adipocytes

undergo hyperplasia and hypertrophy during obesity (Boroumand and Klip, 2020; Doucette et al., 2015; Scheller et al., 2015; Tratwal et al., 2020) we contemplated that this process might be temporally and potentially causally related to the HFD-driven BM myelopoiesis and Ly6C^{high} monocytosis. Finally, we considered whether the response of the monocytic lineage to the BM environment during obesity includes a metabolic shift leading to the increase in Ly6C^{high} monocytes. In fact, and surprisingly, little is known about the metabolic orientation of the Ly6C^{high} monocytes in states of obesity, although there is mounting evidence of a link between a macrophage-intrinsic metabolic shift and their pro-inflammatory orientation in this condition (O'Neill et al., 2016; Sharma et al., 2020; Thapa and Lee, 2019; Verdeguer and Aouadi, 2017).

Hence, the overall hypothesis driving this study is that, with obesity, the increased production of Ly6C^{high} monocytes in the BM is accompanied and possibly caused by a glycolytic shift in these cells, driven by changes in bone marrow adipocytes (BMA). Accordingly, we investigated the temporality of enhanced BM myelopoiesis, BM Ly6C^{high} monocyte accumulation, and AT macrophage changes during high fat diet (HFD) feeding in mice. Next, we explored the potential causal relationship between the obesity-induced changes in BMA and increased Ly6C^{high} monocyte production. Using an *in vitro* platform, we deconstructed the effects of obesity-induced BM cellular changes on Ly6C^{high} monocyte expansion. We report that BM Ly6C^{high} monocytes accumulate in the BM prior to the gain in pro-inflammatory AT macrophages. The rise in BM monocytes temporally correlated with the elevation in BMA. Moreover, BMA whitening correlated with the timely increases in BM Ly6C^{high} monocytes, and most notably, isolated BMA from HFD-fed mice directly favoured Ly6C^{high} monocyte development *ex vivo*. This monocyte developmental change was also induced *ex vivo* by *bona fide* white adipocytes while *bona fide* brown adipocytes favoured Ly6C^{low} monocyte predominance. Notably, the conversion of Ly6C^{low} to Ly6C^{high} monocytes was preceded by a switch in their metabolism, from oxidative to glycolytic. Mechanistically, white adipocytes induced conversion of Ly6C^{low} to Ly6C^{high} monocytes, whereas brown adipocytes increased Ly6C^{low} monocyte proliferation. We propose that HFD-induced changes in BMA disrupts the normal balance of BM monocyte subsets leading to a higher output of tissue invasive Ly6C^{high} monocytes.

93 **Results**

94 **Increased fasting blood glucose, peripheral and BM adiposity by 3 weeks of HFD**

95 To study the temporal relationship of HFD-induced myeloid changes in the BM relative to that in
96 epididymal white AT (EWAT), C57BL/6 mice were fed HFD or control low fat diet (LFD) for either 3, 8
97 or 18 weeks. HFD-fed mice had higher body weight and impaired fasting blood glucose by 3 weeks,
98 compared to controls (**Figure 1A,B**). Body weight and hyperglycemia continued to rise with prolonged
99 feeding. HFD-fed mice also displayed higher EWAT weight (**Figure 1C**) and inter-scapular brown AT
100 (BAT) weight at 3 weeks (not shown). Cross-sectional tibia and femur bone histology visualized via H &
101 E and Oil Red O staining revealed an increase in BMA size by 3 weeks and an increase in BMA number
102 by 8 weeks of HFD (**Figure 1D-G**). This indicated that 3 weeks of HFD sufficed to induce whole body
103 metabolic disturbance and augmented adiposity in peripheral tissues and in the BM.

104 **BM monocytes increase prior to accumulation of EWAT macrophages and monocytes with HFD**

105 Although total EWAT weight increased by 3 weeks, myeloid cells in the stromal vascular fraction
106 (SVF) of AT did were not elevated until 8 weeks of HFD, as revealed by gene expression of the general
107 myeloid marker *Itgam* (encoding CD11b) and monocyte markers $Gr1^-$ $CD115^+$ $CD11b^+$ $Ly6C^+$ (determined
108 by flow cytometry) (**Figures 2A,D**). Similarly, AT macrophages, assessed by gene expression of the AT
109 macrophage marker *Adgre1* (encoding F4/80) and by flow cytometry counting of $CD11b^+$ $Ly6C^-$ $F4/80^+$
110 macrophages in the SVF were not elevated at 3 weeks of HFD but were at 8 weeks (**Figure 2B,E**). Further,
111 gene expression of the pro-inflammatory myeloid marker *Itgax* (encoding CD11c) and surface detection of
112 the pro-inflammatory markers $CD11b^+$ $Ly6C^-$ $F4/80^+$ $CD11c^+$ were also higher in the SVF by 8 weeks of
113 HFD relative to control diet, but not at 3 weeks (**Figure 2C,F**). Of note, gene expression of the
114 embryonically-conserved tissue-resident AT macrophage markers *Timd4* and *Marco* (Beattie et al., 2016;
115 Gibbings et al., 2015) was not elevated at 3 or at 8 weeks and only rose at 18 weeks of HFD (**Figure 2G-**
116 **H**). This indicates that the gain in AT macrophages at 8 weeks of HFD is unlikely due to proliferation of
117 resident macrophages and instead likely results from monocyte recruitment from the circulation.

118 In the BM, total monocytes, gated via the Gr1$^-$ CD115$^+$ CD11b$^+$ Ly6C$^+$ markers, increased at 3
119 weeks and continued to rise by 8 and 18 weeks of HFD (**Figure 2I**). Using the surface abundance of the
120 Ly6C protein as well as the CX3CR1 and CCR2 markers (Auffray et al., 2007, 2009; Kratofil et al., 2017),
121 we subcategorized Ly6C^{low} and Ly6C^{high} monocyte subsets. At 3 weeks into the feeding study, Ly6C^{low} and
122 Ly6C^{high} monocytes represented about 40% of the total BM monocyte population in the control diet group,
123 whereas HFD promoted a higher proportion of Ly6C^{low} monocytes (**Figure 2J**). However, by 8 weeks of
124 HFD there was a marked switch, whereby the relative proportion of Ly6C^{low} monocytes in the total
125 monocyte population was *lower* and that of Ly6C^{high} monocytes was *higher* than under the control diet
126 (**Figure 2J**). These differences were more prominent by 18 weeks of HFD feeding (**Figure 2J**).
127 Collectively, these findings revealed that, in the BM, HFD favoured monocytosis at 3 weeks, with a
128 subsequent and prominent skewing towards tissue invasive Ly6C^{high} monocytes at 8 weeks that continued
129 into 18 weeks of HFD. Singer et al. also demonstrated an increase in BM monocytosis and elevated
130 monocyte precursor cells with 18 weeks of HFD, that persisted after BM transplantation into chow-fed
131 recipients (Singer et al., 2014). In the present study, while we clearly recorded an earlier and continuing
132 rise in total monocytes in HFD-fed mice (**Figure 2I**), we did not observe statistically significant increases
133 in monocyte precursor and stem cells at any time point analyzed (**Figure S1A-C**).

134 **Glycolytic metabolic reprograming in monocyte subsets with HFD**

135 Recent discoveries have highlighted the importance of glycolytic metabolism in the activation of
136 AT macrophages with HFD (Lee and Murphy, 2019), but the metabolic status of monocytes in obesity has
137 not been reported, although some studies have investigated the metabolism of circulating human
138 CD14$^+$CD16$^-$ monocytes (homologous to murine tissue invasive Ly6C^{high} monocytes) during aging (Lee
139 and Murphy, 2019; Pence and Yarbro, 2019). To assess whether HFD affects the metabolic status of BM
140 monocyte subsets in obesity, we analyzed Ly6C^{low} and Ly6C^{high} from control and HFD mice at 3, 8 and 18
141 weeks of feeding. The mitochondrial activity-indicator dye MitoTracker Red CMXRos was incorporated
142 into the monocyte flow cytometry panel (Table 1). MitoTracker Red CMXRos is recruited to the

143 mitochondrial membrane proportionally to the degree of mitochondrial membrane potential and is thus an
144 indicator of mitochondrial activity in oxidative phosphorylation. The results revealed that Ly6C^{low}
145 monocytes have a higher mitochondrial membrane potential than Ly6C^{high} monocytes in the control mice
146 (**Figure 3A-C**). Notably, 3 weeks of HFD reduced the mitochondrial membrane potential in both monocyte
147 subsets indicated by the left-ward shift in the MitoTracker Red CMXRos peak (**Figure 3A**). The HFD-
148 induced effects were more pronounced by 8 and 18 weeks of HFD (**Figure 3B,C**). To further understand
149 the effects of HFD on the developing BM monocytes, Ly6C^{low} and Ly6C^{high} monocytes from mice fed
150 control or HFD for 3, 8 or 18 weeks were isolated via fluorescent activated cell sorting (FACS) and plated
151 for metabolic analysis with a Seahorse XF Analyzer. The results revealed a gradual lowering in the oxygen
152 consumption rate (OCR) of Ly6C^{low} monocytes with HFD (**Figure 3D-I**). Comparison of the area under
153 the curve (AUC) revealed that at 18 weeks, the OCR of the Ly6C^{low} monocytes was significantly lowered
154 with HFD (**Figure 3I**). Interestingly, at 8 and 18 weeks, the AUC of the OCR of the Ly6C^{low} monocytes
155 was significantly higher than the AUC of the OCR of Ly6C^{high} monocytes in the control group (**Figure 3H-**
156 **I**). Moreover, this difference was lost in the HFD group as the AUC of the OCR of Ly6C^{low} monocytes
157 diminished (**Figure 3H-I**).

158 Comparison of the various sections of the OCR graph revealed that the changes in OCR observed
159 with 3 weeks of HFD were not manifest at basal respiration nor at the ATP-dependent respiration, rather
160 they were evident in the maximal respiratory capacity portion of the metabolic stress test (**Figure 3D**). A
161 drop in basal respiration of both monocyte subsets emerged with 8 weeks of HFD and became more
162 pronounced with 18 weeks of HFD (**Figure 3E-F**). This showcased the sustained effects of HFD on
163 monocyte metabolic status. Conversely, the extracellular acidification rate (ECAR) of Ly6C^{low} monocytes
164 was higher than that of Ly6C^{high} monocytes, consistent with a more active metabolism in the former (**Figure**
165 **3J**). However, this difference was lost with HFD, as ECAR dropped in the Ly6C^{low} monocytes and rose in
166 the Ly6C^{high} monocytes relative to the control diet group (**Figure 3J**). Overall, these results suggest that,
167 along with promoting the preponderance of Ly6C^{high} monocytes, HFD also lowers OCR in Ly6C^{low}
168 monocytes.

169 Notably, an analysis of the BM revealed elevated lactate levels across all HFD time points (**Figure**
170 **3K**). This increase in lactate may be due to the glycolytic shift in BM monocytes described above, among
171 other potential sources within the BM cellular composition. Further analysis of the BM soluble fraction
172 failed to evince any changes between control and 18-week HFD-fed mice in pro-inflammatory cytokines
173 TNFα, IL-1*β*, IL-6, CXCL1 or CCL2 (**Figure S2A-C**). Similarly, there were no differences between diet
174 groups in pro-inflammatory gene expression of *IL-6*, *IL-1β* or *Itgax* in FACS-sorted Ly6C^{low} and Ly6C^{high}
175 monocytes (Not Shown). However, *TNFα* gene expression was higher in FACS-sorted Ly6C^{high} monocytes
176 from 18-week HFD-fed mice compared to controls (**Figure S2D**). Collectively, these findings reveal that
177 HFD alters the BM metabolic micro-environment with little effect on pro-inflammatory cytokine secretion
178 (based on the panel tested).

179 **Expression of mitochondrial fusion and fission genes are altered monocytes with HFD**

180 The efficiency of mitochondrial function is largely reliant on its structure. Mitochondria are highly
181 dynamic in structure, largely regulated by concentration of proteins that control fission and fusion (Gottlieb
182 and Bernstein, 2017). Dynamic transitions are closely aligned to metabolic performance. To further assess
183 the mitochondrial activity of monocytes, we enquired whether their expression of mitochondrial dynamic
184 genes is altered with HFD compared to the control group.

185 The analyzed genes involved in mitochondrial fusion were *Mfn1*, *Mfn2*, *Opa1*, *Tomm20* and
186 *Tomm40*, while those involved in mitochondrial fission were *Drp1*, *CypD* and *Fis1*. BM monocytes from
187 mice fed HFD for 3 weeks did not present with differences in gene expression in the tested mitochondrial
188 fusion genes compared to control diet counterparts (**Figure 4A**). BM monocytes isolated from mice fed
189 HFD for 8 weeks showed downregulated *Mfn1* and *Mfn2* compared to the controls (**Figure 4B**). BM
190 monocytes isolated from 18 week HFD-fed mice downregulated the mitochondrial fusion genes *Mfn2*,
191 *Opa1*, and *Tomm20* (**Figure 4C**). Furthermore, from the tested mitochondrial fission genes, *Drp1* was
192 upregulated in the BM monocytes of 3 weeks HFD-fed mice (**Figure 4D**). *Drp1* and *CypD* were also
193 upregulated in BM monocytes of 8 weeks HFD-fed mice (**Figure 4E**). At 18 weeks, all three tested

194 mitochondrial fission genes, *Drp1*, *CypD* and *Fis1* were upregulated (**Figure 4F**). This gene expression
195 pattern suggests that HFD skews the monocyte gene expression to favour downregulation of genes involved
196 in mitochondrial fusion and upregulation of genes involved in fission.

197 Given that Ly6C^{low} and Ly6C^{high} monocytes presented with differences in metabolic preference
198 (glycolytic and oxidative, respectively), and the known link of glycolytic metabolism with mitochondria
199 fragmentation and conversely oxidative metabolism to mitochondrial fusion, we assessed whether the
200 expression patterns of the genes governing mitochondrial fission and fusion would correlated distinctly
201 with the BM monocyte subset abundance in control and HFD-fed mice. Indeed, and notably, the abundance
202 of the Ly6C^{high} monocyte subset negatively correlated with *Mfn2* and positively correlated with *Drp1* levels
203 (**Figure 4G-H**). In contrast, the abundance of BM Ly6C^{low} monocytes did not correlate with the expression
204 patterns of either *Mfn2* or *Drp1* (**Figure 4G-H**). These data are consistent with our metabolic findings
205 suggesting Ly6C^{high} monocytes are more glycolytic and adopt a gene expression pattern that would promote
206 mitochondrial fragmentation.

207

208 **A shift in BMA type at 8 weeks of HFD influences monocyte subset preference and mitochondrial**
209 **dynamic gene expression**

210 Hematopoietic myeloid cells reside in specific niches of the BM that determine their cellular
211 interaction with other co-resident BM cells (Boroumand and Klip, 2020). BMA, while representing a unique
212 type of adipocytes, respond to obesity with an increase their white adipocyte-like fat storing properties and
213 a decrease in brown-like characteristics (Ambrosi et al., 2017; Doucette et al., 2015; Krings et al., 2012;
214 Scheller et al., 2016). To explore the temporal relation of BMA whitening in relation to the development
215 of monocyte subsets, we followed the gene expression of a suite of recently identified markers that are good
216 differentiators of adipocyte types (Nascimento et al., 2014; Ussar et al., 2014) in isolated BMA from femur
217 and tibia of control and HFD-fed mice. By 3 weeks into HFD, the white adipocyte marker Asc1 (encoding
218 the guanine nucleotide-binding protein subunit beta-like protein) was significantly higher and the brown

219 adipocyte marker P2rx5 (encoding purinergic receptor P2X) trended to be lower albeit without reaching
220 statistical significance, relative to control diet. White adipocyte markers *Lep* (leptin) and *AdipoQ*
221 (adiponectin) as well as the brown adipocyte markers *Ucp1* (UCP1) and *Pat2* (Integrin alpha pat-2) did not
222 change (**Figure 5A**). By 8 weeks of HFD, *Asc1* mRNA remained elevated and *Lep* and *AdipoQ* trended in
223 the same direction (**Figure 5B**). Brown adipocyte markers *P2rx5* and *Ucp1* in the isolated BMA of HFD
224 mice were markedly lower relative to those from control diet mice (**Figure 5B**). Thus, 8 weeks of HFD
225 sufficed to shift BMA towards white adiposity. By 18 weeks of HFD, all white adipocyte markers genes
226 showed were upregulated while brown adipocyte markers were downregulated compared to the control
227 group (**Figure 5C**). Analyses of adipocyte differentiation and progenitor cell markers were conducted in
228 the BM pelleted fraction. *Hoxc8*, a regulator of adipocyte progenitors (Nakagami, 2013), was significantly
229 upregulated at 8 weeks along with *Hoxc9* at 18 weeks of HFD (**Figure S3B,C**). The beige adipocyte
230 progenitor marker *Tmem26* was not significantly higher at any of the tested HFD durations (**Figure S3A-**
231 **C**). Expression of the brown adipocyte determinant genes *Tbx1* and *Lhx8* was undetectable in the isolated
232 BMA. Thus, during the course of HFD, while markers for white adipocyte progenitor cells were
233 upregulated, precursors of beige/brown adipocytes were not affected.

234 The rise in BM Ly6C^{high} monocytes and the shift in BMA whitening both manifested by 8 weeks
235 of HFD. Correlative analysis was performed for both Ly6C^{low} and Ly6C^{high} with the white adipocyte marker
236 *Asc1* and the brown adipocyte marker *Ucp1*. The results revealed a significant positive correlation (P value
237 of 0.0123) for Ly6C^{high} monocytes with *Asc1* gene expression (**Figure 5D**). Conversely, the surge in
238 Ly6C^{high} monocytes presented a significant negative correlation (P value of 0.0415) relative to *Ucp1* gene
239 expression (**Figure 5E**). Changes in Ly6C^{low} monocytes did not significantly correlate with *Asc1* (P value
240 of 0.0768) or *Ucp1* (P value of 0.1299) (**Figure 5D-E**). Collectively, the above data suggest the possibility
241 that the mere shift in BMA towards white adiposity may directly favour induction of BM Ly6C^{high}
242 monocytes. To test this hypothesis, we generated conditioned media (CM) from BMA (BMA-CM) pooled
243 from three control and three HFD-fed mice, collected 3, 8 and 18 weeks into the diets. In parallel, BM of
244 control mice was used to generate monocytes through a 5-day *in vitro* differentiation protocol. These

245 monocytes were treated with BMA-CM from control and HFD-fed mice for 18 hours thereafter.
246 Subsequently, the monocyte population was analyzed via flow cytometry. BMA-CM from 3 weeks HFD-
247 fed mice had no effect on the monocyte subset proportions compared to BMA-CM from control diet-fed
248 mice (**Figure 5F**). Strikingly, however, BMA-CM from 8-week HFD-fed mice applied to BM-derived
249 monocytes from control mice resulted a significant production of Ly6C^{high} monocytes compared to the
250 effect of BMA-CM from mice on the 8-week control diet (**Figure 5G**). This skewing was further enhanced
251 when exposing the control BM cells to BMA-CM from 18-week HFD-fed mice (**Figure 5H**).

252 Lastly, we tested whether BMA-CM was capable to induce changes in gene expression of the
253 mitochondrial fusion and fission genes in monocytes, as observed with monocytes isolated from HFD-fed
254 mice. Accordingly, *in vitro-generated* monocytes were treated with BMA-CM from control and HFD-fed
255 mice. As before, the analyzed genes involved in mitochondrial fusion were *Mfn1*, *Mfn2*, *Opa1*, *Tomm20*
256 and *Tomm40*, while the tested genes involved in mitochondrial fission were *Drp1*, *CypD* and *Fis1*.
257 Monocytes treated with BMA-CM from HFD-fed mice for 18 weeks showed significant downregulated
258 mitochondrial fusion genes *Mfn2*, *Tomm20* and *Tomm40* (**Figure 5I**). Conversely, the mitochondrial fission
259 genes *Drp1* and *CypD* were significantly up-regulated in monocytes treated with HFD-derived BMA-CM
260 (**Figure 5J**).

261 These results not only show that HFD-derived BMA-CM can skew monocyte subset cellularity but
262 also can alter mitochondrial morphology via changes in mitochondrial dynamic gene expression. These
263 changes can have consequential effects on the metabolic properties on the monocytes.

264 **White adipocytes favour Ly6C^{high} monocytes and promote mitochondrial fragmentation**

265 To assess whether the effects of BMA on monocyte subset skewing and metabolic differences can
266 be attributed to BMA whitening, we designed a proof of concept experiment studying the influence of *bona*
267 *fide* white or brown adipocytes on monocyte subset determination and metabolic changes *ex vivo*. Isolated
268 adipocytes from EWAT and brown adipocyte tissue (BAT) of three mice were pooled to generate white AT
269 adipocytes (WATA) and brown AT adipocytes (BATA), respectively. Confirming the phenotype of the

270 isolated cells, classical white adipocytes markers were solely expressed in the isolated WATA and classical
271 brown adipocyte markers were exclusively expressed in the BATA (**Figure S3D-E**). The isolated WATA
272 and BATA were cultured for 24 hours and the corresponding CM were collected for subsequent monocyte
273 treatment. BM-derived monocytes from chow-fed mice were treated with WATA-CM, BATA-CM or left
274 untreated. The proportion of Ly6C^{low} and Ly6C^{high} monocyte subsets was determined by flow cytometry
275 analysis (**Figure S4A-C**). This *in vitro* paradigm allowed for direct mechanistic analysis of the influence
276 of white or brown adipocytes on monocytes. These results indicate that WATA-CM favoured Ly6C^{high}
277 monocyte predominance, while BATA-CM propitiated Ly6C^{low} monocyte abundance (**Figure 6A-B**),
278 revealing a novel, differential influence of white and brown adipocytes on monocyte orientation preference.
279 Moreover, CCR2 surface receptors also increased in the monocytes incubated with WATA-CM (Not
280 Shown), validating the effects of white adipocytes in promoting an abundance of tissue invasive Ly6C^{high}
281 monocytes.

282 Since segregated Ly6C^{low} and Ly6C^{high} monocyte subsets had different metabolic orientations, we
283 investigated if the differential adipocyte influence on monocyte subset development corresponded to a
284 change in their metabolic status. To this end, *in vitro*-generated monocytes were treated with WATA-CM,
285 BATA-CM or left untreated for the last 18 hours of the monocyte differentiation protocol. The
286 mitochondrial membrane potential was assessed using MitoTracker Red CMXRos and flow cytometry
287 analysis. Remarkably, Ly6C^{low} monocytes incubated *in vitro* with WATA-CM experienced a left-ward shift
288 in MitoTracker Red CMXRos peak revealing a reduction in mitochondrial membrane potential induced by
289 the WATA-CM (**Figure 6C**), reproducing what was observed with monocytes from HFD-fed mice (see
290 **Figure 3A-C**). Furthermore, the gene expression of mitochondrial fusion genes *Mfn1*, *Mfn2*, *Tomm20* and
291 *Tomm40* were reduced in monocytes treated with WATA-CM (**Figure 6D**). The mitochondrial fission
292 genes *Drp1*, *CypD* and *Fis1* were up-regulated in monocytes treated with WATA-CM (**Figure 6E**).
293 Conversely, treating monocytes with BATA-CM downregulated the mitochondrial fission gene *CypD*
294 (**Figure 6E**). To explore if the changes in mitochondrial fusion and fission gene expression correlated with
295 the corresponding mitochondrial morphology, we utilized super-resolution microscopy to image the

296 mitochondrial protein TOM20 in *in vitro* monocytes adhered to coverslips. Compared to control-medium
297 treated monocytes, WATA-CM induced a striking mitochondrial fragmentation while BATA-CM
298 promoted a more complete mitochondrial elongation (**Figure 6F**). These observations suggest that white
299 adipocytes, which favour Ly6C^{high} monocyte abundance, can alter the metabolic status of Ly6C^{low}
300 monocytes by reducing their mitochondrial membrane potential and altering mitochondrial dynamic gene
301 expression and morphology, thereby linking changes in BMA whitening to monocyte metabolic status.

302 **White and brown adipocytes influence monocytes through distinct mechanisms**

303 Finally, we investigated the mechanisms whereby monocytes undergo the change in subsets in
304 response to *bona fide* white and brown adipocyte media. Although we had not detected HFD-induced
305 changes in hematopoietic stem and monocyte precursor cells *in vivo*, we re-assessed the abundance of these
306 populations upon exposing *in vitro*-generated monocytes to WATA-CM and BATA-CM. The abundance
307 of hematopoietic stem and monocyte precursor cells was determined using appropriate surface markers and
308 flow cytometry analysis (**Table 1, Figure S4D**). A gain in myeloid precursor cell (CMP) was observed in
309 response to WATA-CM treatment (**Figure S5A-C**). However, no differences in the abundance of CD117+,
310 Sca1+, Sca1-, GMP and MEP cells were detected (**Figure S5A-C**). Given these results we investigated
311 other mechanisms by which monocyte subsets may be altered in response to WATA-CM and BATA-CM.

312 We first explored whether the proportion of monocyte subsets was altered through conversion of
313 one subset to another. Ly6C^{high} monocytes have been shown to give rise to Ly6C^{low} monocytes in mouse
314 blood and BM, and this is paralleled by the human homologous CD14 and CD16 monocyte subsets (Kratofil
315 et al., 2017; Lessard et al., 2017; Patel et al., 2017). However, while there has been speculation about the
316 conversion of Ly6C^{low} to Ly6C^{high} monocytes, there is little experimental evidence for this phenomenon.
317 To explore this possibility, we first separately isolated Ly6C^{low} and Ly6C^{high} monocytes through FACS.
318 Each FACS-sorted homogenous monocyte population was treated with WATA-CM, BATA-CM or left
319 untreated for 18 hours. Following treatments, we evaluated the presence of the alternative monocyte
320 subtype relative to that in the respective starting homogenous populations. Surprisingly, no conversion from

321 Ly6C^{high} to Ly6C^{low} monocytes was observed in any condition (**Figure 7A-F**), but, remarkably, there was
322 conversion of the FACS sorted Ly6C^{low} into Ly6C^{high} monocytes following exposure to WATA-CM
323 (**Figure 7B,E**). While the FACS-sorted starting cells were all Ly6C^{low} monocytes, following the 18-hour
324 WATA-CM treatment the monocyte population consisted of 49.7% Ly6C^{high} monocytes (only Ly6C^{low}
325 monocytes 50.3%) (**Figure 7E**). This was in stark contrast to all other isolated cell and CM treatment
326 combinations tested, which gave rise to a maximum of 16.3% of the opposite monocyte subset compared
327 to the starting population. These results revealed the interesting phenomenon of Ly6C^{low} into Ly6C^{high}
328 monocyte conversion induced by white adipocytes.

329 Monocyte precursor cells in the BM and their derivative macrophages in the tissues maintain their
330 cell numbers by cell proliferation (Cassado et al., 2015). Thus, we asked whether proliferation might
331 contribute to the higher proportion of terminally differentiated Ly6C^{high} or Ly6C^{low} monocyte subsets
332 observed following treatment with WATA-CM (in addition to the conversion of Ly6C^{low} into Ly6C^{high}) or
333 BATA-CM, respectively. To this end, we treated BM-generated monocytes with WATA-CM, BATA-CM
334 or left them untreated for 18 hours, with or without the presence of bromodeoxyuridine (BrdU). Using flow
335 cytometry analysis, DNA-incorporated BrdU was detected in the Ly6C^{low} or Ly6C^{high} monocyte gates of
336 the CD11b versus Ly6C plots, with BrdU as the third colorimetric axis. BrdU incorporation is illustrated
337 by a scale of yellow to red hues compared to the corresponding cells not exposed to BrdU. Proliferating
338 cells were quantified as percentage of CD11b^{+} Ly6C^{+} cells that were highly positive for BrdU incorporation.
339 Interestingly, BATA-CM increased DNA-incorporated BrdU in the sorted Ly6C^{low} monocyte subset,
340 present as yellow to red hues in the CD11b^{+} Ly6C^{low} cell gate (**Figure 7G**). This treatment with BATA-
341 CM increased the number of proliferating cells by 25-fold (**Figure 7H**). In contrast, BrdU incorporation in
342 the sorted Ly6C^{high} monocytes did not change with any treatment conditions. These findings revealed that
343 brown adipocytes promote an abundance of Ly6C^{low} monocytes by inducing their proliferation. Moreover,
344 this replicative behavior is consistent with recent findings that proliferative cells have higher glucose
345 consumption, lactate excretion and oxidative phosphorylation relative to quiescent cells (Yao et al., 2019).

346 **Discussion**

347 In this study, we demonstrate a temporal correlation between HFD-induced whitening of BMA and
348 a BM myeloid lineage bias towards Ly6C^{high} monocytes *in vivo*. The latter present a more glycolytic
349 metabolism underpinned by a reduction in mitochondrial membrane potential, a rise in mitochondrial
350 fission genes and a reduction in mitochondrial fusion genes. Causatively, we show that CM from BMA of
351 HFD-fed mice promotes the generation of Ly6C^{high} monocytes *ex vivo.* Phenocopying the effect of BMA
352 derived from HFD-fed mice, *bona fide* WATA favoured a Ly6C^{high} monocyte preponderance, while BATA
353 promoted a dominance of Ly6C^{low} monocytes. Interestingly, these differential influences by the respective
354 adipocytes are induced by distinct cellular pathways. Mechanistically, white adipocytes induced conversion
355 of Ly6C^{low} to Ly6C^{high} monocytes, while brown adipocytes favoured Ly6C^{low} predominance by inducing
356 their proliferation. These changes in monocytes were underpinned by alterations in the monocytes
357 metabolism, as WATA blunted the monocyte's mitochondrial membrane potential and OCR. Overall, our
358 findings reveal a regulation of monocyte subsets directly influenced by adipocytes, whether from the BM
359 or from AT. Along with the observation of dynamic whitening of BMA during HFD, our results contribute
360 to the emerging evidence that BMA are not mere space fillers, rather they are important contributors to
361 cellular metabolism and hematopoietic lineage decisions (Boroumand and Klip, 2020). That these changes
362 occur early on in the course of diet-induced obesity suggests that the BM is an early responder to a change
363 in feeding status and that adipocytes play a significant role in directing monocyte subset skewing.
364 Moreover, they reveal novel mechanisms regulating the genesis of such skewing.

365 **BM as an early sensor and an active contributor to HFD-induced AT macrophage accumulation**

366 It is now widely recognized that many factors contribute to the accumulation of macrophages in
367 AT that includes the contribution of monocytes. There is mounting evidence for both HFD-induced EWAT
368 monocyte chemo-attraction and for enhanced BM myelopoiesis, that work together to increase the
369 monocyte infiltration and pro-inflammatory AT macrophage accumulation (Singer et al., 2014; Trottier et
370 al., 2012 and Fig. 1D-H). Singer *et al.* demonstrated that transplantation of BM from 18-week HFD-fed

371 mice into control recipients increased the number of invasive circulating monocytes and pro-inflammatory
372 AT macrophages (Singer et al., 2014). These findings support the notion that HFD influences hematopoietic
373 myeloid skewing in the BM upstream of monocyte tissue invasion, thereby contributing to downstream
374 systemic and peripheral tissue inflammation. Furthermore, HFD-driven chemoattracting signals from the
375 homeostatically-disrupted EWAT initiate tissue influx and depletion of invasive Ly6C^{high} monocytes from
376 the circulation, which in turn may acts as a signal for their increased production in the BM (Kamei et al.,
377 2006; Nagareddy et al., 2014; Nov et al., 2013; Renovato-Martins et al., 2017).

378 In the present study, by analyzing chronological changes in EWAT and BM myeloid composition,
379 we observed that total BM monocytes increase by 3 weeks of HFD, whereas the proportion of Ly6C^{high}
380 monocyte predominance was evident only at 8 weeks coinciding with a gain in AT macrophages that were
381 also pro-inflammatory skewed. We did not observe statistical significance in HFD-dependent changes in
382 myeloid precursors, likely due to their scarcity since HSC make up only 0.01% of the entire BM nucleated
383 cells (Challen et al., 2009). The rise in total monocytes observed at 3 weeks of HFD and prior to elevation
384 of AT macrophages identifies the BM as an earlier-responding *locus* during HFD. Interestingly, the increase
385 was only apparent in Ly6C^{low} patrolling monocytes and not the Ly6C^{high} tissue invasive monocyte subset
386 that is known for tissue infiltration in chronic obesity. This might be explained by an initial non-specific
387 upregulation of total myelopoiesis and an increased Ly6C^{high} monocyte BM extravasation. Therefore, it
388 appears that only Ly6C^{low} monocytes are elevated in the BM at 3 weeks of HFD. By 8 weeks of HFD, we
389 observed a shift in the monocyte subset proportion, favouring Ly6C^{high} monocytes. Thus, by 8 weeks, the
390 BM has adopted the 'typical' HFD-induced hematopoietic phenotype, in so far as it already shows the
391 increased Ly6C^{high} monocytes previously reported at the habitually studied 16-18 weeks of HFD.
392 Importantly, we detected a gain in pro-inflammatory AT macrophages by 8 weeks of HFD that is concurrent
393 with the predominance of invasive Ly6C^{high} monocytes in the BM. In contrast, the embryonic-derived tissue
394 resident AT macrophage markers, *Timd4* and *Marco* (Beattie et al., 2016; Gibbings et al., 2015), were not
395 elevated until 18 weeks of HFD. This brings to light the importance of the contribution of the BM-derived
396 myeloid cell pool to early EWAT pathology and AT macrophage accumulation.

397 **Changes in BMA influence monocyte subset skewing**

398 BMA are a distinctive member of the BM cellular suite that is sensitive to HFD effects (Pham et
399 al., 2020). In lean mice, BMA present characteristics that are similar to those of beige or brown adipocytes
400 in peripheral AT (Cuminetti and Arranz, 2019). With HFD, BMA undergo hyperplasia and hypertrophy
401 triggered by PPARγ activation (Rosen and MacDougald, 2006). Furthermore, with obesity, adipocyte
402 precursor mesenchymal stem cells tilt their lineage commitment towards adipogenesis (Silva et al., 2016).
403 While BMA are now known to be a distinct adipocyte population, they express several characteristics of
404 white and brown adipocytes (Boroumand and Klip, 2020; Krings et al., 2012; Sulston and Cawthorn, 2016;
405 Tratwal et al., 2020). Brown adipocyte markers of BMA are reduced in obese mice and a parallel adoption
406 of more white adipocyte markers has been observed (Adler et al., 2014b; Doucette et al., 2015; Krings et
407 al., 2012). The amalgamation of upregulated white adipocyte proteins and elevated fat storage capacity is
408 known as BM adipocyte whitening. Obesity-induced gains in whole body adiposity was causally linked to
409 elevated circulating $CD11b^{+}$ monocytes (Takahashi et al., 2003). However, the influence of BMA from
410 either lean or obese mice on the expansion of $CD11b^{+}$ monocytes had not been previously investigated.

411 The limited spatial capacity of the BM interior as well as the proximity of the cellular lineages in
412 the various BM niches lead us to anticipate that the obesity-linked BMA whitening would influence the
413 monocytic lineage. Here, we found a temporal, positive link between BMA hypertrophy and monocytosis
414 at 3 weeks of HFD. By 8 weeks of HFD, BMA whitening also positively correlated with the rise in tissue
415 invasive $Ly6C^{high}$ monocytes in the BM. Interestingly, these findings were not associated with changes in
416 pro-inflammatory signals in either monocyte subset. As a proof of concept for a direct and distinctive
417 influence of adipocytes on monocyte number and subsets, we show that exposure to soluble factors from
418 *bona fide* white adipocytes favours $Ly6C^{high}$ monocyte preponderance while exposure to soluble factors
419 from brown adipocytes favours $Ly6C^{low}$ monocytes. Mechanistically, we discovered that white adipocytes
420 induced conversion of $Ly6C^{low}$ to $Ly6C^{high}$ monocytes, a process that is not well understood at present.
421 Brown adipocytes however induce their influence on $Ly6C^{low}$ monocytes by increasing their proliferation.
422 Interestingly, secretome studies have reported that BAT-derived VEGFA and VEGFB can stimulate

423 proliferation in adipocyte progenitors and endothelial cells (Bagchi et al., 2013; Leung et al., 1989).
424 Adipocyte-specific VEGFA transgenic mice were protected from the effects of HFD and presented altered
425 macrophage polarization (Elias et al., 2012). Therefore, it is conceivable that a reduction in brown adipocyte
426 characteristics of BMA also leads to a drop in the factors that would normally favour proliferation of
427 Ly6C^{low} monocytes. While the identification of the soluble unknown factor(s) responsible for the adipocyte-
428 specific myeloid influence is outside the focus of the present study, we have laid the foundation for a future,
429 comprehensive investigation of the molecular mediators involved.

430 **How do adipocytes skew myeloid lineage subsets?**

431 While the designation of macrophages as 'M1 and M2' (of pro- or anti-inflammatory
432 characteristics, respectively) represents the extremes of a wide spectrum of phenotypes, the 'M1' pro-
433 inflammatory orientation has been linked to glycolytic activation while the 'M2' anti-inflammatory
434 orientation has been linked to oxidative phosphorylation (Castoldi et al., 2016; Kelly and O'Neill, 2015).
435 A similar glycolytic metabolic switch with obesity has been reported for CD8 pro-inflammatory T cells
436 (Buck et al., 2017). Surprisingly, while pro-inflammatory pathways in monocytes are activated by
437 hyperglycemic conditions (Shanmugam et al., 2003), the metabolic preference of the different monocyte
438 subsets had not been explored. This is a compelling question, given that Ly6C^{high} monocytes penetrate
439 tissues and differentiate to pro-inflammatory 'M1' AT macrophages while Ly6C^{low} monocytes enter tissues
440 to promote healing and repair (Geissmann et al., 2003; Lin et al., 2009). Therefore, we hypothesized here
441 that, in the context of metabolic inflammation, there is a change in the metabolic phenotype of monocyte
442 subsets.

443 Our findings show that Ly6C^{high} and Ly6C^{low} monocytes had different metabolic preferences at
444 baseline, with Ly6C^{low} having higher mitochondrial membrane potential indicative of more active oxidative
445 phosphorylation. Interestingly, HFD consumption lowered the mitochondrial membrane potential of both
446 Ly6C^{low} and Ly6C^{high} monocytes, implicating a reduction in their mitochondrial oxidative capacity. This
447 change aligned with a HFD-induced reduction in oxygen consumption by Ly6C^{low} monocytes. Importantly,

448 this difference was observed as early as 3 weeks and exacerbated by 8 and 18 weeks of HFD. The elevated
449 lactate concentration measured in the BM at all HFD durations may be reflective of metabolic changes in
450 cells of the BM cavity. Since we did not observe changes in the lactate levels in WATA-CM or BATA-
451 CM, the higher lactate in BM of HFD-fed mice may not originate from changes in BMA.

452 Along with the change in monocyte subset proportions, we observed an increase in genes
453 responsible for mitochondrial fragmentation and a decrease in those involved in mitochondrial elongation
454 in monocytes from HFD-fed mice and treated with WATA-CM and BMA-CM. The physiological
455 consequence of these changes was revealed by the observation of a striking mitochondrial fragmentation in
456 monocytes treated with WATA-CM in comparison to control or BATA-CM treated monocytes. HFD is
457 known to induce mitochondrial fission in a number of cells that correlates with insulin resistance. A recent
458 report linked the two phenomena through *Drp1* action, as *Drp1* inhibition reversed HFD-induced insulin
459 resistance (Filippi et al., 2017). Furthermore, obese and diabetic humans have reduced *Mfn2* expression in
460 skeletal muscle. *Mfn2* positively correlates with insulin sensitivity (Bach et al., 2005), and *Mfn2* gene and
461 protein are significantly downregulated in liver cells of HFD-fed rats (Gan et al., 2013). In our analysis, the
462 expression of *Mfn2* negatively correlated with the abundance of Ly6C^{high} monocytes, while, the expression
463 of *Drp1* positively correlated with the BM abundance of Ly6C^{high} monocytes. Overall, our findings reveal
464 novel and distinct effects of adipocyte types on monocyte subset development that may occur through
465 changes in mitochondrial fitness.

466 Given that the proportion of Ly6C^{low} monocytes dropped in favour of a predominance of Ly6C^{high}
467 monocytes by 8 but not 3 weeks of HFD, it is possible that this subset change obeys a prior shift in their
468 metabolic orientation. Supporting these observations, exposure of monocytes to white adipocyte CM also
469 reduced their mitochondrial membrane potential. Furthermore, BMA-CM from 8-week HFD-fed mice also
470 lowered monocyte mitochondrial membrane potential compared to control BMA-CM and favoured
471 Ly6C^{high} predominance. Mechanistically, these data suggest that white adipocytes induce a monocyte
472 metabolic shift that may guide Ly6C^{high} monocyte prevalence.

473 In conclusion, we demonstrate an interconnectivity of cellular networks within the BM, a
474 vulnerability of the BM microenvironment to HFD, and a consequential myeloid lineage determination
475 likely due to BMA whitening. Given the vastly different metabolic and soluble factors between *bona fide*
476 white and brown adipocytes, it is easy to imagine that phenotypic changes in BMA can vastly alter the BM
477 microenvironment and the factors that surround hematopoietic cells. BMA whitening during HFD feeding
478 contributes to myelopoiesis and predominance of invasive Ly6C^{high} monocytes mediated by changes in
479 monocyte metabolism.

480 **Materials and Methods**

481 **Animal Procedures**

482 Mouse protocols were approved by the animal care committee (Protocol #20011850 to S.E.G. and
483 D.J.P., University of Toronto and #1000047074 to A.K., The Hospital for Sick Children). Three groups of
484 9-week-old male C57BL/6 mice were fed either low fat diet (10% kcal from fat; D12450Ji, Research Diets)
485 or HFD (60% kcal from fat; D12492i, Research Diets) for 3, 8, or 18 weeks. Mice were singly caged to
486 avoid stress and weight inequalities induced by aggression of the dominant male to the subordinate male
487 (Kappel et al., 2017). The cages were maintained at 22°C on a 12h light/dark cycle, the diets were replaced
488 once per week and various cage enrichments were provided including switching the positioning of the cages
489 throughout the study.

490 Body weight was measured twice per week. Upon completion of the respective feeding durations,
491 mice were fasted for 4 hours, blood was drawn via tail vein and fasting blood glucose was measured with
492 a glucometer. Mice were euthanized by cervical dislocation. Tissues were dissected and flash frozen in
493 liquid nitrogen for RNA isolation. EWAT, blood and BM were immediately processed for flow cytometry
494 analysis.

495 **EWAT-Derived Stromal Vascular Fraction (SVF) Isolation**

496 EWAT-derived SVF was collected as previously described (Orr et al., 2013). Excised EWAT was
497 rinsed in PBS, minced and digested with 0.47wv/mL Liberase solution (Millipore Sigma, Cat No
498 5401054001) shaking at 200 rpm for 20 mins at room temperature. SVF was isolated using a 70 µm cell
499 strainer, the enzymatic activity of Liberase was neutralized with DMEM containing HI-FBS for 5 minutes
500 and centrifuged at 500 ×g for 10 minutes. The supernatant containing adipocytes was removed, the pellet
501 was re-suspended in red blood cell lysis buffer for 5 minutes to remove erythrocytes and washed with PBS
502 three times.

503

504 **BM Histology**

505 Extracted tibia and femur bones were fixed in 10% formalin for 48 hours, decalcified in 14% EDTA
506 solution for 14 days, paraffin wax-embedded, and longitudinal sections were stained with H&E and Oil
507 Red O (Millipore Sigma; Cat No O0625) to visualize BM adiposity.

508 **BM-Derived Monocyte Suspension Cell Culture and Differentiation**

509 Murine primary BM cells were plated at 500,000 cells/mL on Thermo Scientific™ Nunc™ Non-
510 Treated 6-well plates (Cat No 1256680) with complete RMPI (company) and supplemented with
511 recombinant mouse M-CSF (Peprotech Inc. Cat No 315-02) at 20ng/mL for 5 days (Francke et al., 2011).
512 Following 5 days of BM cell incubation on the ultra-low attachment surface plates, the suspended cells
513 have the signature of mature monocytes and can be used for experimentation. These BM-derived
514 differentiated monocytes were then collected, washed with RMPI, centrifuged and re-suspended with
515 various adipocyte CM for 18 hours.

516 **Primary Adipocyte Isolation and Culture**

517 Epididymal white and interscapular brown AT were dissected in sterile conditions, the tissues
518 underwent mechanical mincing and enzymatic digestion by collagenase type I (Worthington Biochemical
519 Corp, Cat No LS004197) at 4mg/mL shaking for 1 hour. The digested adipocytes were then filtered through
520 a 200 µm cell strainer and centrifuged, washed twice and plated in adipocyte media: high glucose DMEM,
521 1% BSA, 0.5% FBS, and 1% Penicillin and Streptomycin for 24 hours. BM adipocytes were isolated from
522 the floating fraction following BM isolation via centrifugation. The cells were counted and cultured in
523 adipocyte media overnight. Tissues from three mice were collected and the isolated cells were pooled in
524 each CM generating experiment.

525 **Flow Cytometry**

526 Following red blood cell lysis, SVF, blood and the BM were washed with FACS buffer, stained
527 with Aqua Live/Dead Antibody (ThermoFisher, L34957) for 15 minutes in the dark, washed with FACS

528 buffer again, blocked with anti-mouse CD16/32 antibody (eBioscience, 14-0161-86) for 15 minutes in the
529 dark following a 30 minutes' incubation with corresponding antibody for each tissue **(Table 1).** The
530 samples were then fixed, read on LSR Fortessa cytometer (BD Biosciences) and data gated based on
531 appropriate fluorescence minus one (FMO) controls and analyzed on the FlowJo software version 10
532 (Becton, Dickinson & Company).

533 **Quantitative PCR (qPCR)**

534 RNA was extracted from cells or tissues using TRIzol™ (Life Technologies, Cat No 15596018),
535 then cDNA synthesized using the SuperScript VILO cDNA kit (Life Technologies, Cat No 11754250)
536 according to manufacturer's instructions. qPCR reactions were performed with predesigned TaqMan probes
537 (Life Technologies) on a StepOne Plus Real-Time PCR System (Life Technologies). Gene expression was
538 normalized to that of housekeeping genes, Abt1, Hprt, and Eef2 by the $\Delta\Delta C_T$ method.

539 **BrdU incorporation**

540 BM derived monocytes were labelled with 10 µM BrdU (abcam, ab6326) during the 18-hour
541 treatment at 37C. The cells were then washed with FACS buffer, surface markers were stained as described
542 above and incubated in Foxp3 Fixation/Permeabilization Buffer (eBioscience, 00-5523-00) overnight. They
543 were then treated with 30 µg of DNAse I.9 (Sigma, 260913). for 1 hour, stained with anti-BrdU antibody
544 for 1 hour and then washed with FACS buffer in preparation to run on LSR Fortessa Cytometer.

545 **Fluorescent Activated Cell Sorting of Monocytes**

546 BM from two femurs and tibias of 10-week-old chow-fed mice was used in the isolation of
547 monocyte subsets via fluorescent activated cell sorting using the FACS Aria Ilu instrument. $Gr1^-$ $CD115^+$
548 $CD11b^+$ $Ly6C^+$ surface markers were used in identifying total monocytes and the two subsets were
549 subsequently distinguished by the relative surface abundance of Ly6C protein. Isolated $Ly6C^{low}$ and
550 $Ly6C^{high}$ monocytes were then validated using antibodies to CX3CR1 and CCR2 (**Table 1**), respectively.

551 **Cell Metabolism Analysis**

552 Oxygen consumption (OCR) and extracellular acidification rates were measured using a Seahorse
553 XFe96 analyzer (Seahorse Bioscience). Seahorse 96-well cell culture plates were pretreated with 1 µg/cm^2
554 Corning™ Cell-Tak Cell and Tissue Adhesive (Fisher Scientific, Cat No CB40240) and FACS sorted
555 Ly6C^{low} or Ly6C^{high} monocytes were seeded at 100,000 cells/well, allowed to equilibrate for 1h in XF base
556 medium supplemented with 11 mM glucose, 1 mM sodium pyruvate and 2mM Glutamine. Following
557 baseline measurements, FCCP was injected at 1mM and thereafter an injection of Antimycin A/ Rotenone.
558 Cells were counted following the seahorse assay to test for changes in cellular detachment between the
559 conditions.

560 **Immunofluorescence Staining for Super-Resolution Microscopy**

561 Monocytes were spun down onto coverslips and fixed with 4% paraformaldehyde for 15 minutes.
562 Thereafter, the cells were rinsed with PBS and permeabilized with 0.1% Triton X-100 for 10 minutes. The
563 cells were then blocked with 2% BSA in PBS at 4℃ overnight. The cells were then incubated with the
564 primary antibody, Tom20 (FL-145, Santa Cruz, sc-11415), in a 1:100 dilution in blocking buffer at 4℃
565 overnight. Thereafter, the cells were incubated with Alexa Fluor 488 anti-rabbit secondary antibody (1:100)
566 for 2 hours at room temperature. Cells were incubated with Alexa Fluor 568 Phalloidin (1:100) for 3 hours
567 at room temperature. Coverslips were then mounted by ProLong Diamond (Thermo Fisher Scientific) and
568 allowed to dry for two days. The images were acquired via Zeiss LSM880 Airyscan super resolution
569 microscopy and the images were processed via Fiji software.

570 **ELISA**

571 The BM content was fractioned into hematopoietic and supernatant portions by centrifugation at
572 1,600 rpm. The supernatant fraction was re-suspended in 500ul of 1X PBS (supplemented with Protease
573 Cocktail Inhibitor, Sigma). Total protein content was estimated by Pierce™ BCA Protein Assay Kit
574 (ThermoFisher Scientific). Subsequently, mouse TNF, IL-1b, IL-6, CXCL1 and CCL2 ELISAs were

575 carried out according to the manufacturers' instructions. All Mouse DuoSet ELISA kits were purchased
576 from R&D systems. The individual protein contents were finally normalised to total protein content.

577 **Statistical Analysis**

578 Data are expressed as means ± SEM. An unpaired Student's T test was used to detect differences
579 in data sets with one variable. A one-way ANOVA with Tukey post-test was used to detect differences in
580 data sets of two or more variables. Statistical significance was set at $P < 0.05$. Data analysis and statistics
581 tests were done using GraphPad Prism version 6 (GraphPad Software), Flow Jo Software version 10.4 and
582 figures were prepared using Adobe Illustrator CS6 version 16.0.

583 **Acknowledgements**

584 A.K. was supported by Canadian Institutes of Health Research (CIHR) Foundation Grant (FND-143203)
585 and D.J.P. was supported by CIHR Foundation Grant (FDN-14333). P.B. was supported by a Banting &
586 Best Diabetes Centre-Novo Nordisk Graduate Studentship from 2017 to 2019 and by a SickKids
587 Restracomp Award from 2019 to 2020. We thank Dr. Clinton Robbins for support with hematopoietic
588 lineage analysis.

589

590 **Author Contribution**

591 P.B., S.E.G. and A.K. conceived the study design. P.B. performed experiments and analyzed the
592 data. M.W., J.S., I.T., N.S., L.Z., Z.L., A.L., T.M. and Y.Z. participated in experimental work and data
593 collection. A.K., D.J.P., and S.E.G. provided access to resources and facilities. P.J.B. contributed with
594 advice and trouble-shooting. P.B. and A.K. wrote the manuscript, and all authors read and approved it.

References:

Adler, B.J., Kaushansky, K., and Rubin, C.T. (2014). Obesity-driven disruption of haematopoiesis and the bone marrow niche. Nat. Rev. Endocrinol. *10*, 737–748.

Ambrosi, T.H., Scialdone, A., Graja, A., Gohlke, S., Jank, A.M., Bocian, C., Woelk, L., Fan, H., Logan, D.W., Schürmann, A., et al. (2017). Adipocyte Accumulation in the Bone Marrow during Obesity and Aging Impairs Stem Cell-Based Hematopoietic and Bone Regeneration. Cell Stem Cell *20*, 771–784.e6.

Auffray, C., Fogg, D., Garfa, M., Gaelle, E., Join-Lambert, O., Kayal, S., Sarnacki, S., Ana, C., Lauvau, G., and Geissmann, F. (2007). Monitoring of Blood Vessels and Tissues by a Population of Monocytes with Patrolling Behavior. *317*, 666–671.

Auffray, C., Fogg, D.K., Narni-Mancinelli, E., Senechal, B., Trouillet, C., Saederup, N., Leemput, J., Bigot, K., Campisi, L., Abitbol, M., et al. (2009). CX 3 CR1 + CD115 + CD135 + common macrophage/DC precursors and the role of CX 3 CR1 in their response to inflammation . J. Exp. Med. *206*, 595–606.

Bach, D., Naon, D., Pich, S., Soriano, F.X., Vega, N., Rieusset, J., Laville, M., Guillet, C., Boirie, Y., Wallberg-henriksson, H., et al. (2005). Expression of Mfn2, the Charcot-Marie-Tooth Neuropathy Type 2A Gene, in Human Skeletal Muscle. Diabetes *54*, 2685–2693.

Bagchi, M., Kim, L.A., Boucher, J., Walshe, T.E., Kahn, C.R., and Amore, P.A.D. (2013). Vascular endothelial growth factor is important for brown adipose tissue development and maintenance. FASEB J. *27*, 3257–3271.

Beattie, L., Sawtell, A., Mann, J., Frame, T.C.M., Teal, B., de Labastida Rivera, F., Brown, N., Walwyn-Brown, K., Moore, J.W.J., MacDonald, S., et al. (2016). Bone marrow-derived and resident liver macrophages display unique transcriptomic signatures but similar biological functions. J. Hepatol. *65*, 758–768.

Boniakowski, A.E., Kimball, A.S., Joshi, A., Schaller, M., Davis, F.M., denDekker, A., Obi, A.T., Moore, B.B., Kunkel, S.L., and Gallagher, K.A. (2018). Murine macrophage chemokine receptor CCR2 plays a crucial role in macrophage recruitment and regulated inflammation in wound healing. Eur. J. Immunol. *48*, 1445–1455.

Boroumand, P., and Klip, A. (2020). Bone marrow adipose cells – cellular interactions and changes with obesity. J. Cell Sci. *1*, 1–8.

Buck, M.D., Sowell, R.T., Kaech, S.M., and Pearce, E.L. (2017). Metabolic Instruction of Immunity. Cell *169*, 570–586.

Cassado, A.A., D'Império Lima, M.R., and Bortoluci, K.R. (2015). Revisiting mouse peritoneal macrophages: Heterogeneity, development, and function. Front. Immunol. *6*, 1–9.

Castoldi, A., De Souza, C.N., Saraiva Câmara, N.O., and Moraes-Vieira, P.M. (2016). The macrophage switch in obesity development. Front. Immunol. *6*, 1–11.

Centers for Disease Control and Prevention, C. (2017). National Diabetes Statistics Report: Estimates of Diabetes and Its Burden in the United States. Atlanta, GA: Centers for Disease Control and Prevention; 2017. US Dep. Heal. Hum. Serv.

Challen, G.A., Boles, N., Lin, K.K.Y., and Goodell, M.A. (2009). Mouse hematopoietic stem cell identification and analysis. Cytom. Part A *75*, 14–24.

Cuminetti, V., and Arranz, L. (2019). Bone Marrow Adipocytes: The Enigmatic Components of the Hematopoietic Stem Cell Niche. J. Clin. Med. *8*, 707.

Doucette, C.R., Horowitz, M.C., Berry, R., MacDougald, O.A., Anunciado-Koza, R., Koza, R.A., and Rosen, C.J. (2015a). A High Fat Diet Increases Bone Marrow Adipose Tissue (MAT) But Does Not Alter Trabecular or Cortical Bone Mass in C57BL/6J Mice. J Cell Physiol *230*, 2032–2037.

642 Doucette, C.R., Horowitz, M.C., Berry, R., Macdougald, O.A., Anunciado-Koza, R., Koza, R.A.,
643 and Rosen, C.J. (2015b). A High Fat Diet Increases Bone Marrow Adipose Tissue (MAT) But
644 Does Not Alter Trabecular or Cortical Bone Mass in C57BL/6J Mice. J. Cell. Physiol. *230*,
645 2032–2037.
646 Elias, I., Franckhauser, S., Ferré, T., Vilà, L., Tafuro, S., Muñoz, S., Roca, C., Ramos, D., Pujol,
647 A., Riu, E., et al. (2012). Adipose Tissue Overexpression of Vascular Endothelial Growth Factor
648 Protects Against Diet-Induced Obesity and Insulin Resistance. Diabetes *61*, 1801–1813.
649 Filippi, B.M., Abraham, M.A., Silva, P.N., Bauer, P. V, Rocheleau, J. V, Lam, T.K.T., Filippi,
650 B.M., Abraham, M.A., Silva, P.N., Rasti, M., et al. (2017). Mitochondrial Fission Changes in the
651 Dorsal Vagal Report Dynamin-Related Protein 1-Dependent Mitochondrial Fission Changes in
652 the Dorsal Vagal Complex Regulate Insulin Action. CellReports *18*, 2301–2309.
653 Fink, L.N., Costford, S.R., Lee, Y.S., Jensen, T.E., Bilan, P.J., Oberbach, A., Blüher, M.,
654 Olefsky, J.M., Sams, A., and Klip, A. (2014a). Pro-Inflammatory macrophages increase in
655 skeletal muscle of high fat-Fed mice and correlate with metabolic risk markers in humans.
656 Obesity *22*, 747–757.
657 Fink, L.N., Costford, S.R., Lee, Y.S., Jensen, T.E., Bilan, P.J., Oberbach, A., Blüher, M.,
658 Olefsky, J.M., Sams, A., and Klip, A. (2014b). Pro-Inflammatory macrophages increase in
659 skeletal muscle of high fat-Fed mice and correlate with metabolic risk markers in humans.
660 Obesity *22*, 747–757.
661 Francke, A., Herold, J., Weinert, S., Strasser, R.H., and Braun-Dullaeus, R.C. (2011). Generation
662 of mature murine monocytes from heterogeneous bone marrow and description of their
663 properties. J. Histochem. Cytochem. *59*, 813–825.
664 Friedrich, K., Sommer, M., Strobel, S., Thrum, S., and Blüher, M. (2019). Perturbation of the
665 Monocyte Compartment in Human Obesity. Front. Immunol. *10*, 1–10.
666 Gan, K., Wang, C., Chen, J., Zhu, C., and Song, G. (2013). Mitofusin-2 ameliorates high-fat diet-
667 induced insulin resistance in liver of rats. *19*, 1572–1581.
668 Garvey, W.T., Henry, R.R., Kern, P.A., Saghizadeh, M., and Ong, J.M. (2008). The expression
669 of TNF alpha by human muscle. Relationship to insulin resistance. J. Clin. Invest. *97*, 1111–
670 1116.
671 Geissmann, F., Jung, S., and Littman, D.R. (2003). Blood monocytes consist of two principal
672 subsets with distinct migratory properties. Immunity *19*, 71–82.
673 Gibbings, S.L., Goyal, R., Desch, A.N., Leach, S.M., Prabagar, M., Atif, S.M., Bratton, D.L.,
674 Janssen, W., and Jakubzick, C. V. (2015). Transcriptome analysis highlights the conserved
675 difference between embryonic and postnatal-derived alveolar macrophages. Blood *126*, 1357–
676 1366.
677 Gottlieb, R.A., and Bernstein, D. (2017). Mitochondrial Remodeling: Rearranging, Recycling,
678 and Reprogramming. Cell Calcium *60*, 88–101.
679 Griffin, C., Eter, L., Lanzetta, N., Abrishami, S., Varghese, M., McKernan, K., Muir, L., Lane,
680 J., Lumeng, C.N.-K., and Singer, K. (2018). TLR4, TRIF, and MyD88 are essential for
681 myelopoiesis and CD11c+ adipose tissue macrophage production in obese mice. J. Biol. Chem.
682 jbc.RA117.001526.
683 Hamann, A. (2017). Obesity Update 2017. Diabetologe.
684 Kamei, N., Tobe, K., Suzuki, R., Ohsugi, M., Watanabe, T., Kubota, N., Ohtsuka-kowatari, N.,
685 Kumagai, K., Sakamoto, K., Kobayashi, M., et al. (2006). Overexpression of Monocyte
686 Chemoattractant Protein-1 in Adipose Tissues Causes Macrophage Recruitment and Insulin
687 Resistance *. J. Biol. Chem. *281*, 26602–26614.

688 Kappel, S., Hawkins, P., and Mendl, M. (2017). To Group or Not to Grou? Good Practice for
689 Housing Male Laboratory Mice. Animals 1–25.
690 Kelly, B., and O'Neill, L.A. (2015). Metabolic reprogramming in macrophages and dendritic
691 cells in innate immunity. Cell Res. *25*, 771–784.
692 Kohyama, M., Matsuoka, S., Shida, K., Sugihara, F., Aoshi, T., Kishida, K., Ishii, K.J., and
693 Arase, H. (2016). Monocyte infiltration into obese and fibrilized tissues is regulated by PILRα.
694 Eur. J. Immunol. *46*, 1214–1223.
695 Kratofil, R.M., Kubes, P., and Deniset, J.F. (2017). Monocyte conversion during inflammation
696 and injury. Arterioscler. Thromb. Vasc. Biol. *37*, 35–42.
697 Krings, A., Rahman, S., Huang, S., Lu, Y., Czernik, P.J., and Lecka-Czernik, B. (2012). Bone
698 marrow fat has brown adipose tissue characteristics, which are attenuated with aging and
699 diabetes. Bone *50*, 546–552.
700 Lanthier, N., Molendi-Coste, O., Horsmans, Y., van Rooijen, N., Cani, P.D., and Leclercq, I.A.
701 (2010). Kupffer cell activation is a causal factor for hepatic insulin resistance. Am. J. Physiol.
702 Liver Physiol. *298*, G107–G116.
703 Lee, M.K.S., and Murphy, A.J. (2019). Glycolysis Is Required for LPS-Induced Activation and
704 Monocytes. *10*, 1–10.
705 Lessard, A.J., LeBel, M., Egarnes, B., Préfontaine, P., Thériault, P., Droit, A., Brunet, A., Rivest,
706 S., and Gosselin, J. (2017). Triggering of NOD2 Receptor Converts Inflammatory Ly6Chighinto
707 Ly6ClowMonocytes with Patrolling Properties. Cell Rep. *20*, 1830–1843.
708 Leung, D.W., Cachianes, G., Kuang, W., Goeddel, D. V, and Ferrara, N. (1989). Vascular
709 Endothelial Growl th Factor Is a Secreted Angiogenic Mitogen. Science (80-.). *246*, 1306–9.
710 Lin, S.L., Castano, A.P., Nowlin, B.T., Lupher, M.L., and Duffield, J.S. (2009). Bone Marrow
711 Ly6Chigh Monocytes Are Selectively Recruited to Injured Kidney and Differentiate into
712 Functionally Distinct Populations. J. Immunol. *183*, 6733–6743.
713 Liu, T., Sun, Y.-C., Cheng, P., and Shao, H.-G. (2019). Adipose tissue macrophage-derived
714 exosomal miR-29a regulates obesity-associated insulin resistance. Biochem. Biophys. Res.
715 Commun.
716 Lumeng, C.N., Deyoung, S.M., Bodzin, J.L., and Saltiel, A.R. (2007). Increased Inflammatory
717 Properties of Adipose Tissue Macrophages Recruited During Diet-Induced Obesity. Diabetes *56*,
718 16–23.
719 Lumeng, C.N., Delproposto, J.B., Westcott, D.J., and Saltiel, A.R. (2008). Phenotypic Switching
720 of Adipose Tissue Macrophages With Obesity Is Generated by Spatiotemporal Differences in
721 Macrophage Subtypes. Diabetes *57*, 3239–3246.
722 Manicone, A.M., Gong, K., Johnston, L.K., and Giannandrea, M. (2016). Diet-induced obesity
723 alters myeloid cell populations in naïve and injured lung. Respir. Res. *17*, 24.
724 Nagareddy, P.R., Kraakman, M., Masters, S.L., Stirzaker, R.A., Gorman, D.J., Grant, R.W.,
725 Dragoljevic, D., Hong, E.S., Abdel-Latif, A., Smyth, S.S., et al. (2014). Adipose tissue
726 macrophages promote myelopoiesis and monocytosis in obesity. Cell Metab. *19*, 821–835.
727 Nakagami, H. (2013). The Mechanism of White and Brown Adipocyte Differentiation. Diabetes
728 Metab. J. *37*, 85–90.
729 Nascimento, E.B.M., Boon, M.R., and van Marken Lichtenbelt, W.D. (2014). Fat cells gain new
730 identities. Sci. Transl. Med. *6*, 1–4.
731 Nov, O., Shapiro, H., Ovadia, H., Tarnovscki, T., Dvir, I., Shemesh, E., Kovsan, J., Shelef, I.,
732 Carmi, Y., Voronov, E., et al. (2013). Interleukin-1β Regulates Fat-Liver Crosstalk in Obesity by
733 Auto-Paracrine Modulation of Adipose Tissue Inflammation and Expandability. PLoS One *8*.

O'Neill, L., Kishton, R., and Rathmell, J. (2016). A guide to immunometabolism for immunologists. Nat. Rev. Immunol. *16*, 553–565.

Orr, J.S., Kennedy, A.J., and Hasty, A.H. (2013). Isolation of Adipose Tissue Immune Cells. J. Vis. Exp. 1–7.

Patel, A.A., Zhang, Y., Fullerton, J.N., Boelen, L., Rongvaux, A., Maini, A.A., Bigley, V., Flavell, R.A., Gilroy, D.W., Asquith, B., et al. (2017). The fate and lifespan of human monocyte subsets in steady state and systemic inflammation. J. Exp. Med. *214*, 1913–1923.

Pence, B.D., and Yarbro, J.R. (2019). Classical monocytes maintain ex vivo glycolytic metabolism and early but not later inflammatory responses in older adults. Immun. Ageing *16*, 1–8.

Pham, T.T., Ivaska, K.K., Hannukainen, J.C., Virtanen, K.A., Lidell, M.E., Parkkola, R., Piirola, S., Oikonen, V., Nuutila, P., Biology, C., et al. (2020). Human bone marrow adipose tissue is a metabolically active and insulin sensitive distinct fat depot. J. Clin. Endocrinol. Metab. *pii*, dgaa216.

Renovato-Martins, M., Matheus, M.E., de Andrade, I.R., Moraes, J.A., da Silva, S.V., Citelli dos Reis, M., de Souza, A.A.P., da Silva, C.C., Bouskela, E., and Barja-Fidalgo, C. (2017). Microparticles derived from obese adipose tissue elicit a pro-inflammatory phenotype of CD16 + , CCR5 + and TLR8 + monocytes. Biochim. Biophys. Acta - Mol. Basis Dis. *1863*, 139–151.

Rosen, E.D., and MacDougald, O.A. (2006). Adipocyte differentiation from the inside out. Nat. Rev. Mol. Cell Biol. *7*, 885–896.

Scheller, E.L., Doucette, C.R., Learman, B.S., Cawthorn, W.P., Khandaker, S., Schell, B., Wu, B., Ding, S.Y., Bredella, M.A., Fazeli, P.K., et al. (2015). Region-specific variation in the properties of skeletal adipocytes reveals regulated and constitutive marrow adipose tissues. Nat. Commun. *6*, 1–13.

Scheller, E.L., Khoury, B., Moller, K.L., Wee, N.K.Y., Khandaker, S., Kozloff, K.M., Abrishami, S.H., Zamarron, B.F., and Singer, K. (2016). Changes in skeletal integrity and marrow adiposity during high-fat diet and after weight loss. Front. Endocrinol. (Lausanne). *7*, 1–13.

Shanmugam, N., Reddy, M.A., Guha, M., and Natarajan, R. (2003). High glucose-induced expression of proinflammatory cytokine and chemokine genes in monocytic cells. Diabetes *52*, 1256–1264.

Sharma, M., Boytard, L., Hadi, T., Koelwyn, G., Simon, R., Ouimet, M., Seifert, L., Spiro, W., Yan, B., Hutchison, S., et al. (2020). Enhanced glycolysis and HIF-1 α activation in adipose tissue macrophages sustains local and systemic interleukin-1 β production in obesity. Sci. Rep. *10*, 1–12.

Silva, S. V, Renovato-martins, M., Ribeiro-pereira, C., Citelli, M., and Barja-fidalgo, C. (2016). Obesity Modifies Bone Marrow Microenvironment and Directs Bone Marrow Mesenchymal Cells to Adipogenesis. Obes. Biol. Integr. Physiol. *24*, 2522–2532.

Singer, K., DelProposto, J., Lee Morris, D., Zamarron, B., Mergian, T., Maley, N., Cho, K.W., Geletka, L., Subbaiah, P., Muir, L., et al. (2014). Diet-induced obesity promotes myelopoiesis in hematopoietic stem cells. Mol. Metab. *3*, 664–675.

De Souza, C.T., Araujo, E.P., Bordin, S., Ashimine, R., Zollner, R.L., Boschero, A.C., Saad, M.J.A., and Velloso, L.A. (2005). Consumption of a fat-rich diet activates a proinflammatory response and induces insulin resistance in the hypothalamus. Endocrinology *146*, 4192–4199.

Sulston, R.J., and Cawthorn, W.P. (2016). Bone marrow adipose tissue as an endocrine organ: close to the bone? Horm. Mol. Biol. Clin. Investig. *28*, 21–38.

780 Takahashi, K., Mizuarai, S., Araki, H., Mashiko, S., Ishihara, A., Kanatani, A., Itadani, H., and
781 Kotani, H. (2003). Adiposity Elevates Plasma MCP-1 Levels Leading to the Increased CD11b-
782 positive Monocytes in Mice *. J. Biol. Chem. *278*, 46654–46660.
783 Thapa, B., and Lee, K. (2019). Metabolic influence on macrophage polarization and
784 pathogenesis. BMB Rep. *52*, 360–372.
785 Tratwal, J., Labella, R., Bravenboer, N., and Kerckhofs, G. (2020). Reporting Guidelines ,
786 Review of Methodological Standards , and Challenges Toward Harmonization in Bone Marrow
787 Adiposity Research . Report of the Methodologies Working Group of the International Bone
788 Marrow Adiposity Society. Front. Endocrinol. (Lausanne). *11*, 1–36.
789 Ussar, S., Lee, K., Dankel, S., Boucher, J., Haering, M., Kleinridders, A., Thomou, T., Xue, R.,
790 Macoteia, Y., Cypess, A., et al. (2014). Asc-1, PAT2 and P2RX5 are novel cell surface markers
791 for white, beige and brown adipocytes. Sci Transl Med *247*, 247ra103.
792 doi:10.1126/scitranslmed.3008490. Asc-1,.
793 Verdeguer, F., and Aouadi, M. (2017). Macrophage heterogeneity and energy metabolism. Exp.
794 Cell Res. *360*, 35–40.
795 Weisberg, S.P., McCann, D., Desai, M., Rosenbaum, M., Leibel, R.L., and Ferrante, A.W.
796 (2003). Obesity is associated with macrophage accumulation in adipose tissue. J. Clin. Invest.
797 *112*, 1796–1808.
798 Weisberg, S.P., Hunter, D., Huber, R., Lemieux, J., Slaymaker, S., Vaddi, K., Charo, I., Leibel,
799 R.L., and Ferrante Jr, A.W. (2006). CCR2 modulates inflammatory and metabolic effects of
800 high-fat feeding. J. Clin. Invest. *116*, 115–124.
801 WHO (2016). World Health Organization. Global Report on Diabetes. Geneva, Switzerland.
802

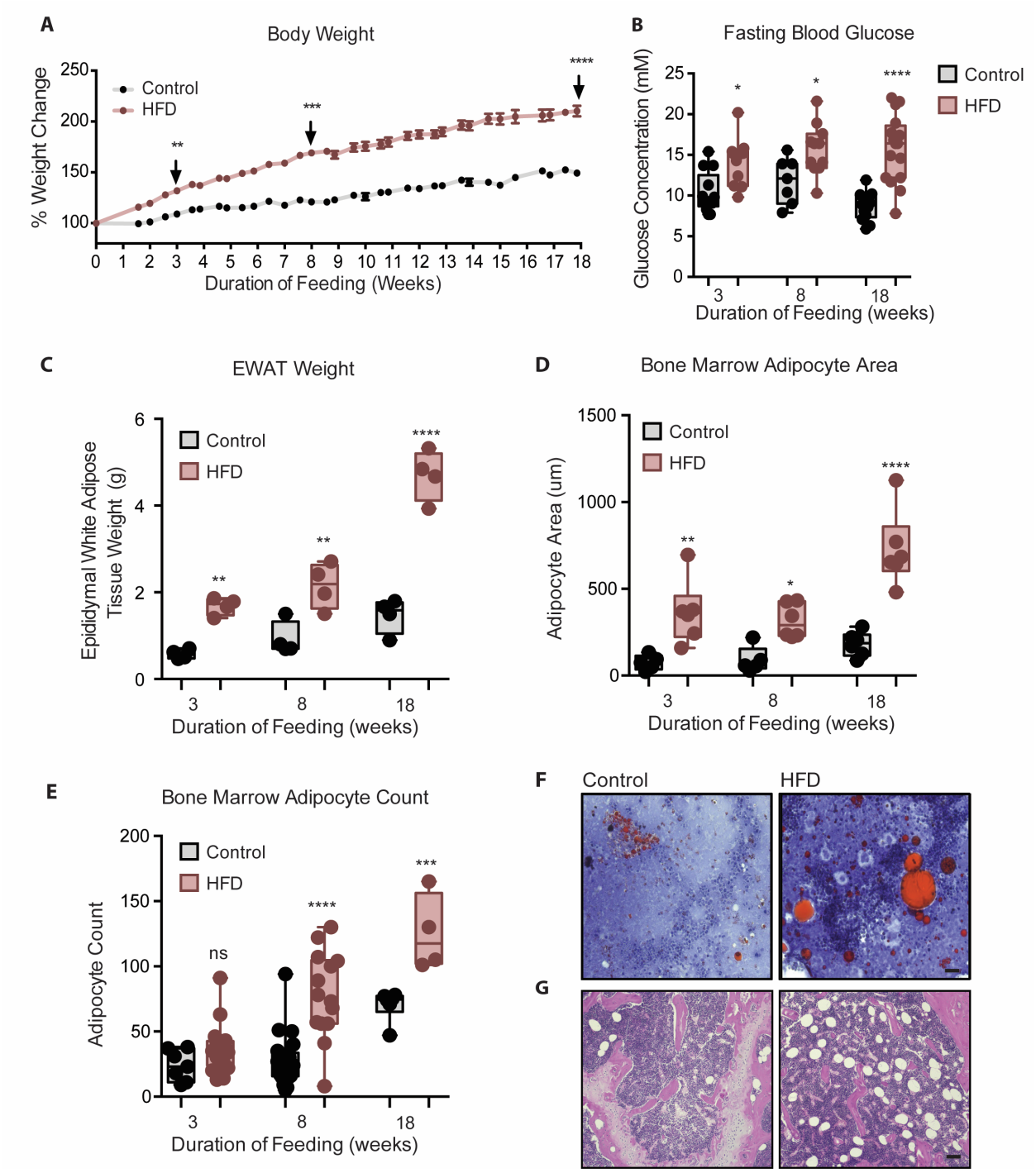

Figure 1. Mice fed HFD increased body weight, fasting blood glucose, visceral and bone marrow adipose tissue. [A] Body weight was measured twice a week throughout the course of feeding. [B] Mice were fasted for 4 hours after which fasting blood glucose was measured. [C] Epididymis white adipose tissue was weighed the day of sacrifice. [D] Area covered by bone marrow adipocytes were measured

808 following hematoxylin and eosin (H&E) to visualize adipocyte ghosts using quantified using ImageJ. [E]
809 Bone marrow adipocyte numbers were blindly counted following H&E staining. [F] Femurs of control
810 and HFD-fed mice were fixed in formalin for 2 days followed by 14 days EDTA decalcification and
811 subsequently stained with ORO and [G] H&E. Scale bar is 25μm. Results are expressed as mean ± SEM,
812 n=4-14 mice per group. One-way ANOVA was used for statistical analysis at each dietary group and
813 across feeding periods. *P < 0.05, **P < 0.01, ***P < 0.001, ****P < 0.0001 and ns = not significant.

Figure 2

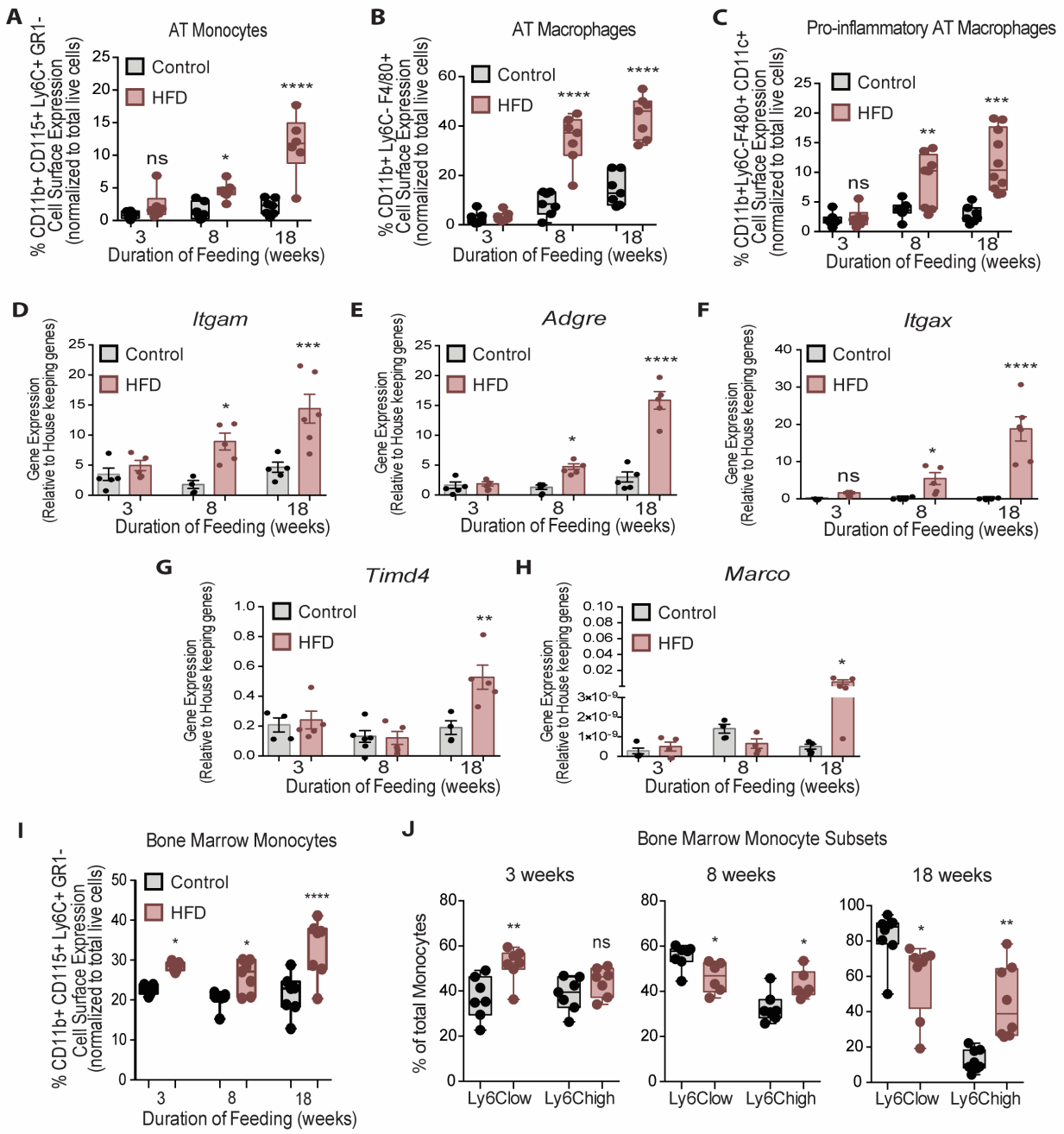

Figure 2. Bone marrow monocytes increased prior to adipose tissue macrophages. Quantification of stromal vascular fraction (SVF) of [A] adipose tissue monocytes [B] total macrophages and [C] pro-inflammatory macrophages via flow cytometry analysis identified first by size and granularity through forward and side scatter and then using the following markers: CD11b CD115 F4/80 Ly6C GR1 CD11c. [D-F] Whole adipose tissue gene expression of the myeloid marker *Itgam,* macrophage marker *Adgre* and

820 pro-inflammatory myeloid marker *Itgax* by RTqPCR. [G-H] Gene expression analysis of embryonic
821 derived tissue resident macrophage markers *Timd4* and *Marco* by RTqPCR. [I] Flow cytometry analysis of
822 total and [J] monocyte subsets in the bone marrow with HFD-feeding. Results are expressed as mean ±
823 SEM, n=5-10 mice per group. One-way ANOVA was used for statistical analysis at each dietary group and
824 across feeding periods. *P < 0.05, **P < 0.01, ***P < 0.001, ****P < 0.0001 and ns = not significant.

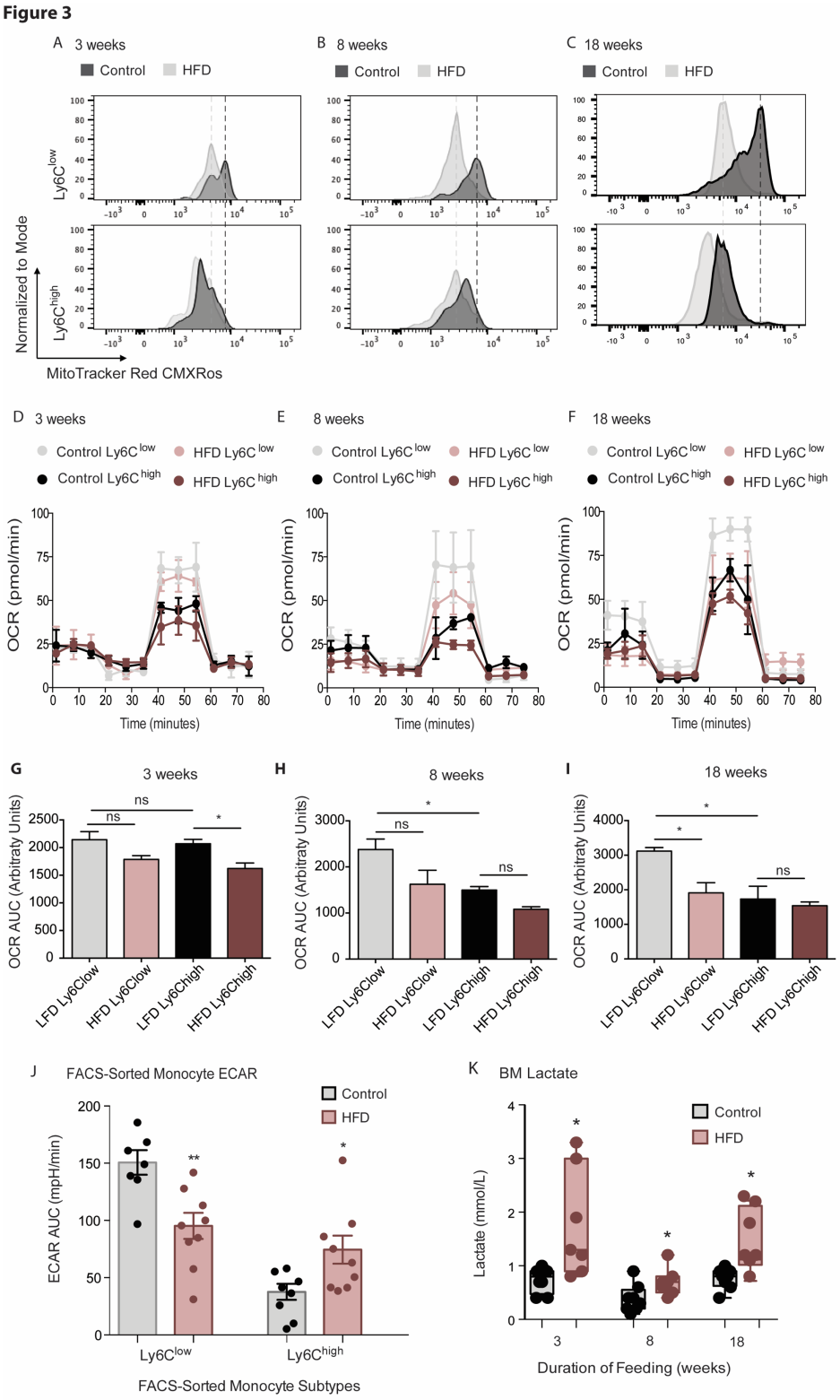

825

826 **Figure 3. HFD blunted the mitochondrial oxidation of monocyte subsets.** Flow cytometry detection of

827 [A-C] MitoTracker Red CMXRos in bone marrow monocyte subsets of control and HFD-fed mice. [D-F]

828 OCR of FACS-sorted Ly6C^{low} and Ly6C^{high} monocytes from control and HFD-fed mice measured by the
829 Seahorse Assay. [G-I] Area under the curve of OCR of FACS-sorted Ly6C^{low} and Ly6C^{high} monocytes from
830 control and HFD-fed mice measured by the Seahorse Assay. [J] Area under the curve of ECAR
831 measurement from FACS-sorted Ly6C^{low} and Ly6C^{high} monocytes of control and HFD-fed mice measured
832 by the Seahorse Assay and pooled from all feeding durations. [K] BM lactate measurement of the
833 supernatant fraction in HFD and control samples. Results are expressed as mean ± SEM, n=3 mice per
834 group where applicable. One-way ANOVA was used for statistical analysis. *$P < 0.05$ and **$P < 0.01$.
835 Graph in panels C was created using FlowJo software (Becton, Dickinson Company).

Figure 4

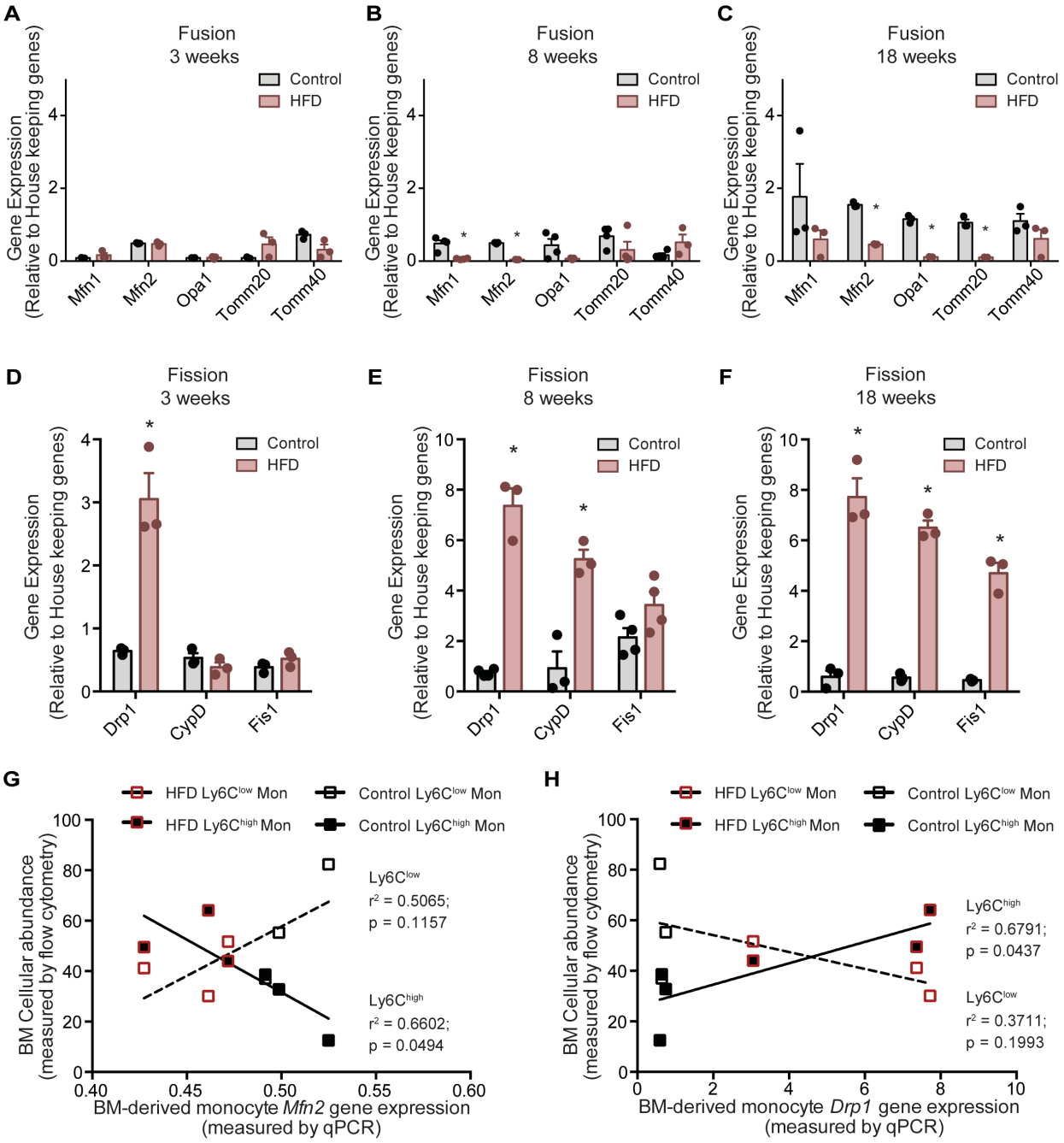

Figure 4. HFD downregulated gene expression of mitochondrial fusion genes and upregulated mitochondrial fission genes. Gene expression of mitochondrial fusion genes *Mfn1, Mfn2, Opa1, Tomm20,* and *Tomm40* in monocytes isolated from control and HFD-fed mice for [A] 3, [B] 8, [C] 18 weeks. Gene expression of mitochondrial fission genes *Drp1, CypD* and *Fis1* in monocytes isolated from control and HFD-fed mice for [D] 3, [E] 8, [F] 18 weeks. [G] Correlative analysis of monocyte subset BM cellular

842 abundance and BM-derived monocyte *Mfn2* gene expression. [H] Correlative analysis of monocyte subset

843 BM cellular abundance and BM-derived monocyte *Drp1* gene expression. Results are expressed as mean ±

844 SEM, n=3-9 mice per group. One-way ANOVA was used for statistical analysis. *$P < 0.05$.

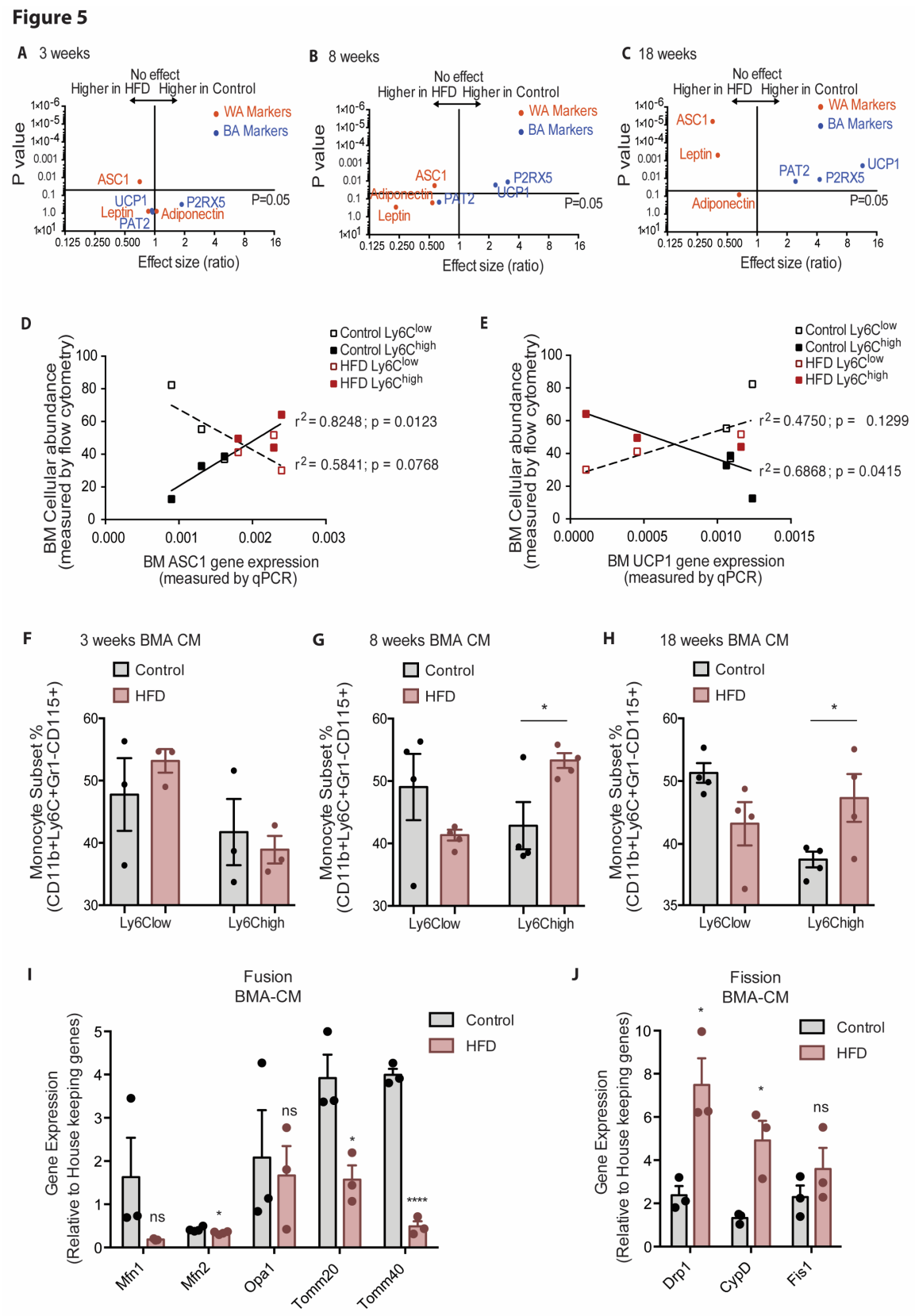

845

846 **Figure 5. Bone marrow adipocyte whitening detected at 8 and 18 weeks of HFD favours increased**

847 **bone marrow Ly6C^{high} monocytes and induced changes in mitochondrial dynamic gene expression.**
848 Volcano plots showing the gene expression of white and brown adipocyte markers in red and blue
849 respectively [A] at 3, [B] 8 and [C] 18 weeks of HFD. Correlative graphs of the [D] white adipocyte marker
850 ASC1 and [E] brown adipocyte marker UCP1 with Ly6C^{low} and Ly6C^{high} monocyte subsets. Flow
851 cytometry quantification of naïve Ly6C^{low} and Ly6C^{high} monocytes upon 18 hours of treatment with BMA-
852 CM from control and HFD-fed mice for [F] 3, [G] 8 and [H]18 weeks. [I] Gene expression of mitochondrial
853 fusion genes *Mfn1, Mfn2, Opa1, Tomm20,* and *Tomm40* in naïve monocytes treated with BMA-CM from
854 control and HFD-fed mice. [J] Gene expression of mitochondrial fission genes *Drp1, CypD* and *Fis1* in
855 naïve monocytes treated with BMA-CM from control and HFD-fed mice. Results are expressed as mean ±
856 SEM, n=3-9 mice per group. One-way ANOVA was used for statistical analysis at each dietary group and
857 across feeding periods. *$P < 0.05$, ****$P < 0.0001$ and ns = not significant.

Figure 6

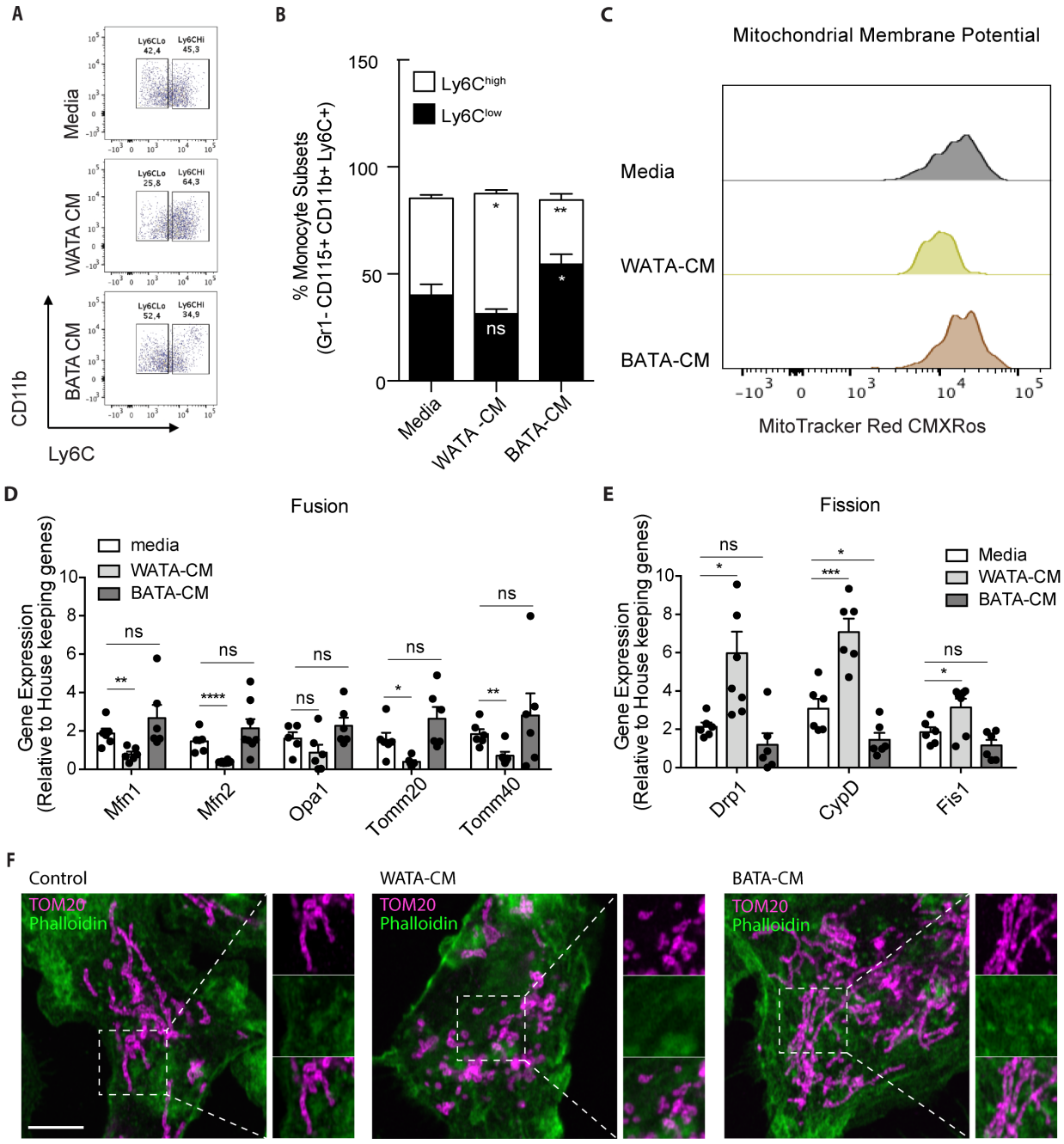

858

859 **Figure 6. *Bona fide* white adipocytes favoured Ly6C^{high} monocytes preponderance, blunted**

860 **monocyte mitochondrial membrane potential, and induced mitochondrial fragmentation *in vitro*.**

861 Naïve monocytes were treated with CM from isolated *bone fide* white and brown adipocytes from EWAT

862 and inter-scapular BAT for 18 hours. [A] Flow cytometry dot plots detecting the effects of 18 hours of

863 treatment with media alone, WATA-CM and BATA-CM on monocyte subset abundance with the [B]
864 quantification of the gates drawn for Ly6C^{low} and Ly6C^{high} monocytes. [C] MitoTracker Red CMXRos
865 detected by flow cytometry in Ly6C^{low} monocytes treated with media alone, WATA-CM and BATA-CM
866 for 18 hours. [D] Gene expression of mitochondrial fusion genes *Mfn1*, *Mfn2*, *Opa1*, *Tomm20*, and
867 *Tomm40* in naïve monocytes treated with Media, WATA-CM and BATA-CM. [E] Gene expression of
868 mitochondrial fission genes *Drp1*, *CypD* and *Fis1* in naïve monocytes treated with Media, WATA-CM
869 and BATA-CM. [F] Super-resolution microscopy analysis of mitochondrial morphology via TOM20
870 staining in monocytes treated with Media, WATA-CM and BATA-CM. Scale bar = $5\mu m$. Images
871 analyzed in Fiji (version 2.1.0/1.53c). WATA-CM = white adipose tissue adipocyte-conditioned media;
872 BATA-CM = brown adipocyte tissue adipocyte-conditioned media. EWAT = epididymal white adipose
873 tissue; BAT = brown adipose tissue. Results are expressed as mean ± SEM, n=3-9 mice per group. One-
874 way ANOVA was used for statistical analysis. *P < 0.05, **P < 0.01 and ***P < 0.001, ****P < 0.0001
875 and ns = not significant. Graphs in panels A-C were created using FlowJo software (Becton, Dickinson
876 Company).

Figure 7

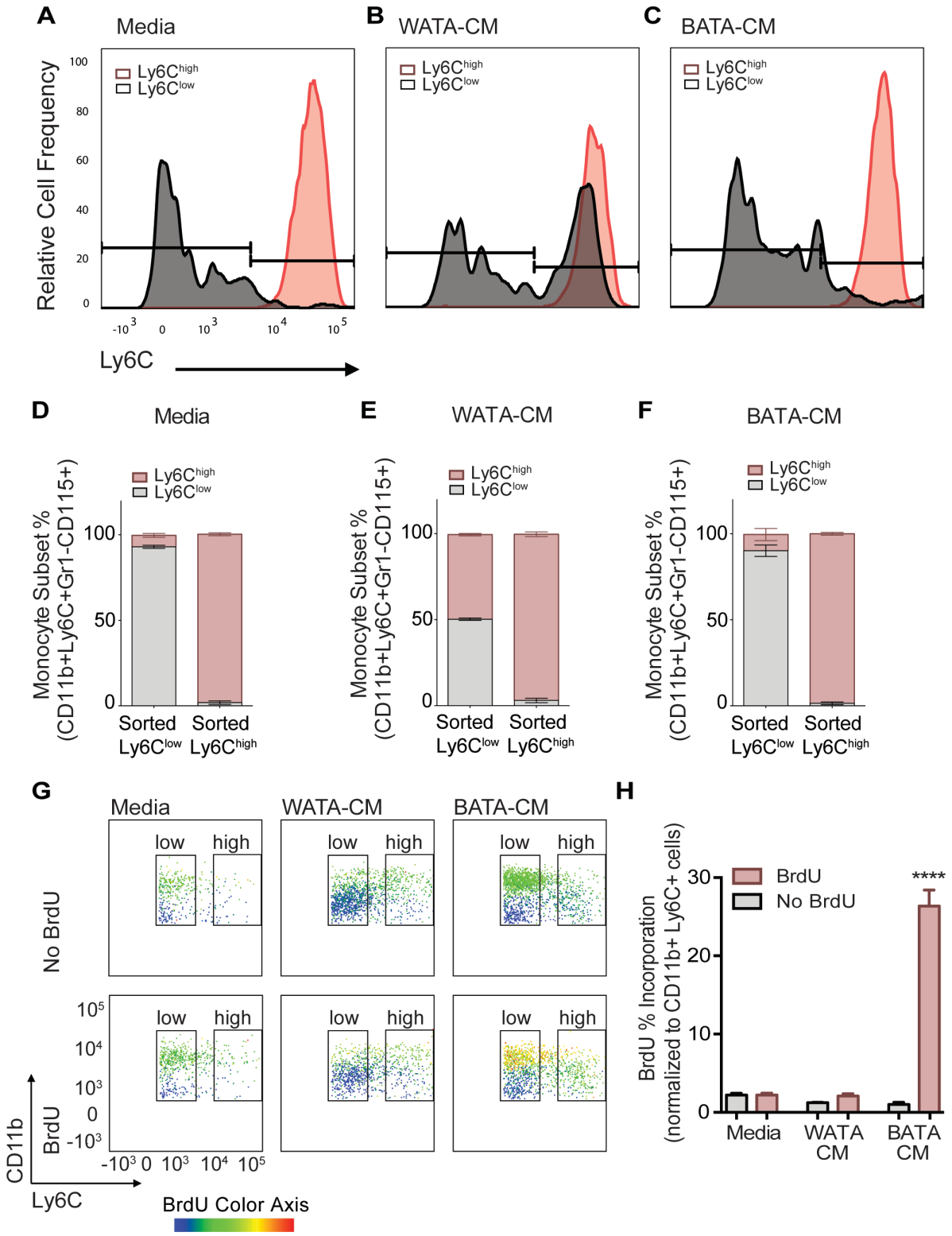

877

878 **Figure 7. White and brown adipocytes favour Ly6C^{high} and Ly6C^{low} monocytes through different**

879 **mechanisms.** FACS-sorted Ly6C^{low} and Ly6C^{high} monocytes from control mice were independently treated
880 with [A] media alone, [B] WATA-CM and [C] BATA-CM for 18 hours after which the presence of the
881 alternate monocyte subset was assessed via flow cytometry. [D-F] Quantification of Ly6C^{low} and Ly6C^{high}
882 gates in panels A-C. [G] *In vitro* generated monocytes were treated with media alone, WATA-CM or
883 BATA-CM in the presence of the pyrimidine analogue BrdU to detect cellular proliferation. [H]
884 Quantification of BrdU abundance in Ly6C^{low} and Ly6C^{high} with treatments in panel C. Results are
885 expressed as mean ± SEM, n=3-6 mice per group. One way ANOVA test was used for statistical analysis.
886 ****$P < 0.0005$. Graphs in panels A-C and G were created using FlowJo software (Becton, Dickinson
887 Company).

888

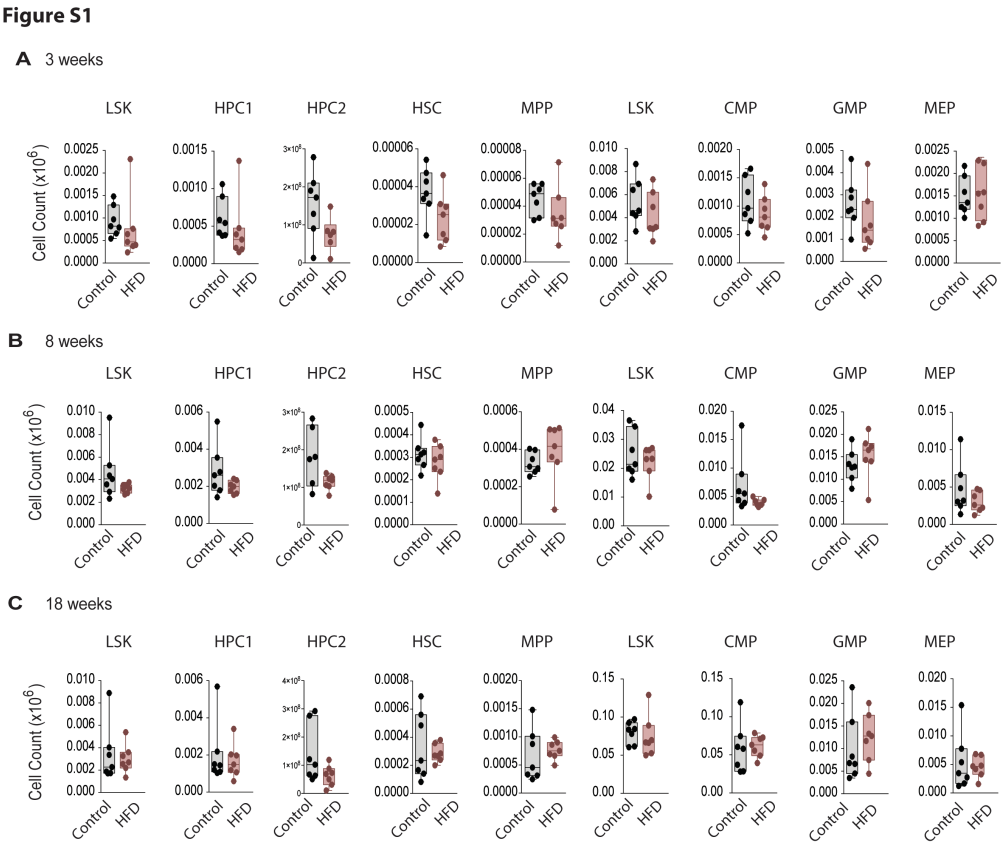

Figure S1. Monocyte precursor and stem cells were not significantly altered with HFD *in vivo*. Flow cytometry analysis of HSC and monocyte precursor cells in mice fed a Control or HFD for [A] 3, [B] 8, and [C] 18 weeks. Flow cytometry antibodies used are listed in Table 1. Student's T test was used and no statistical significance was observed.

Figure S2

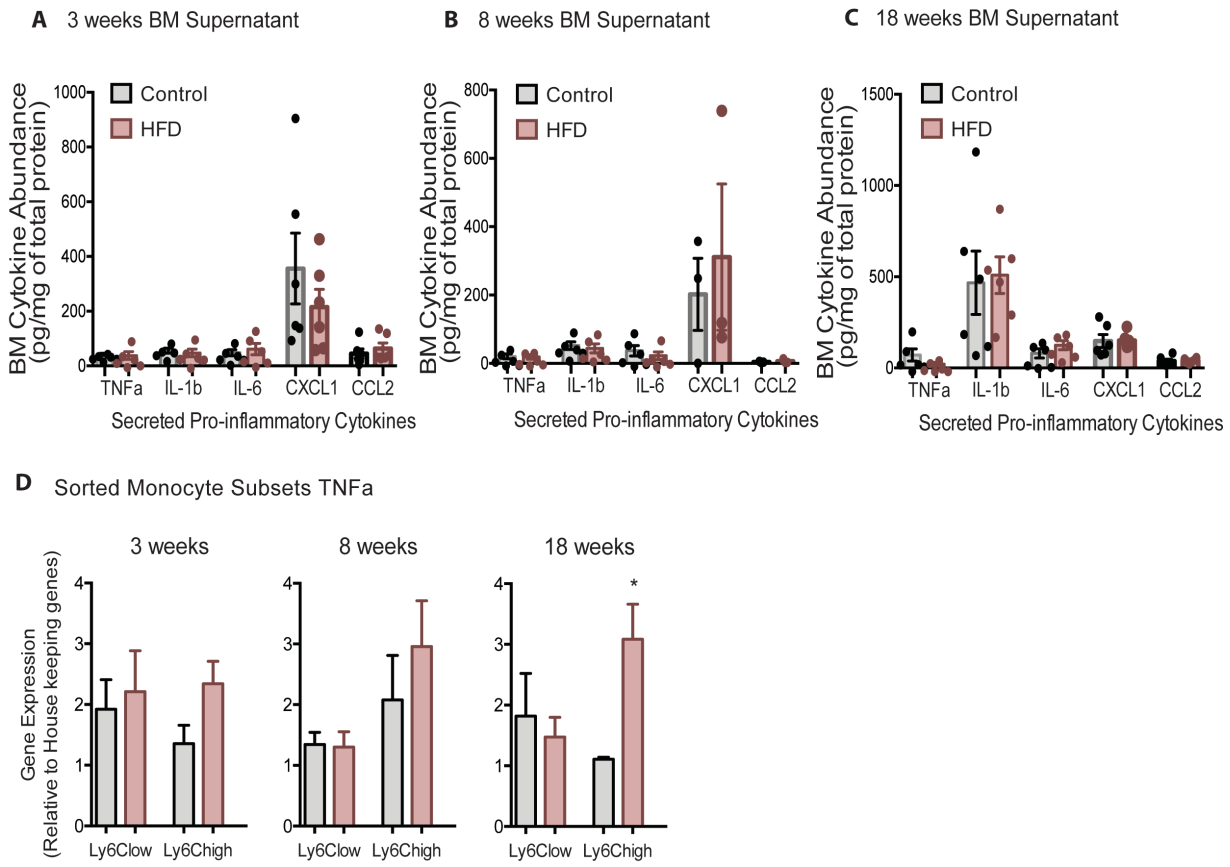

894

895 **Figure S2: BM pro-inflammatory factors did not change with HFD.** No changes in pro-inflammatory
896 cytokines were detected in BM supernatant fraction using the ELISA assay in mice fed control or HFD for
897 [A] 3, [B] 8, or [C] 18 weeks. FACS-sorted monocyte subsets were analyzed for changes in pro-
898 inflammatory gene expression; shown in [D] TNFα gene expression increased with 18 weeks of HFD in
899 Ly6Chigh monocytes but no other changes were detected. Results are expressed as mean ± SEM, n=3-6
900 mice per group. One way ANOVA test was used for statistical analysis. *P < 0.05 and **P < 0.01.

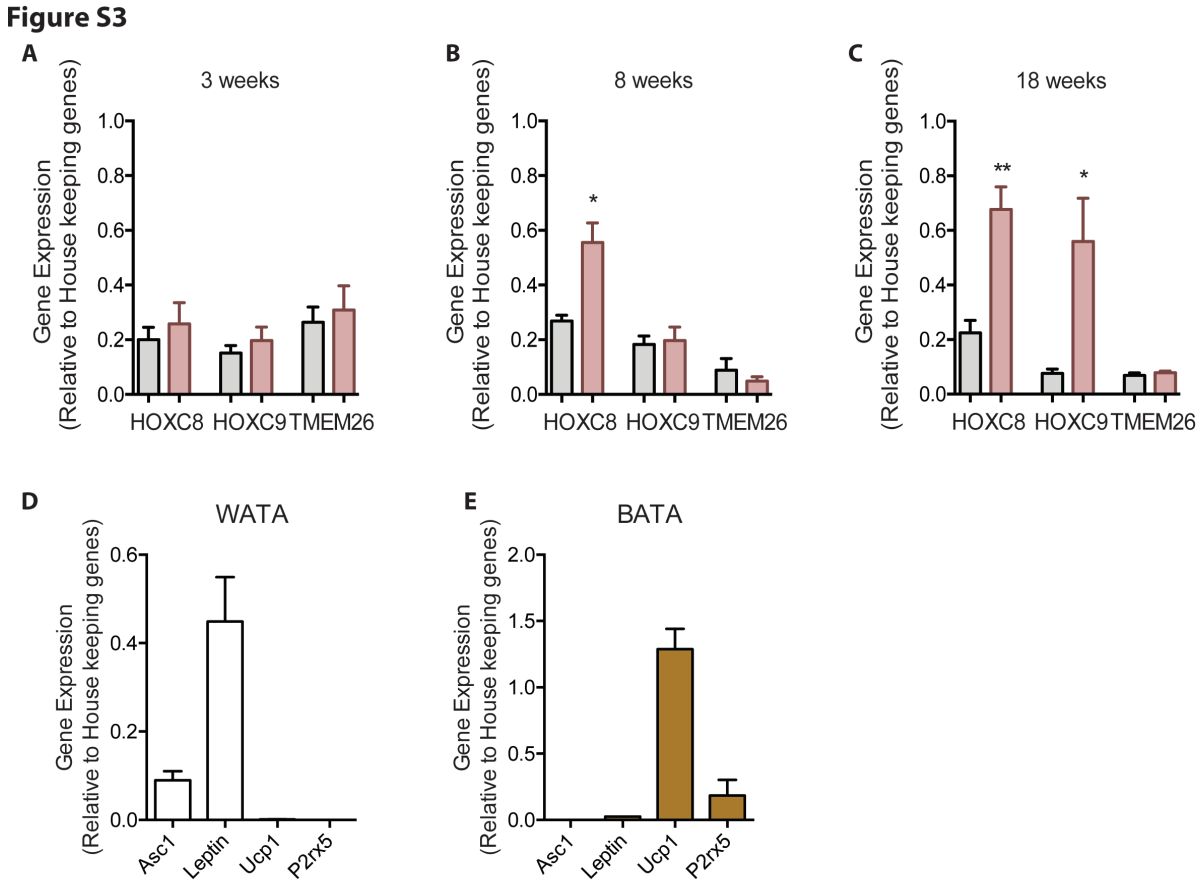

Figure S3. BMA precursor cells with HFD. RT qPCR of isolated pelleted fraction were assessed for pre-adipocyte markers of mice fed a Control or HFD for [A] 3, [B] 8, and [C] 18 weeks. [D] classical white and brown adipocyte markers were confirmed in isolated WATA and BATA.

Figure S4

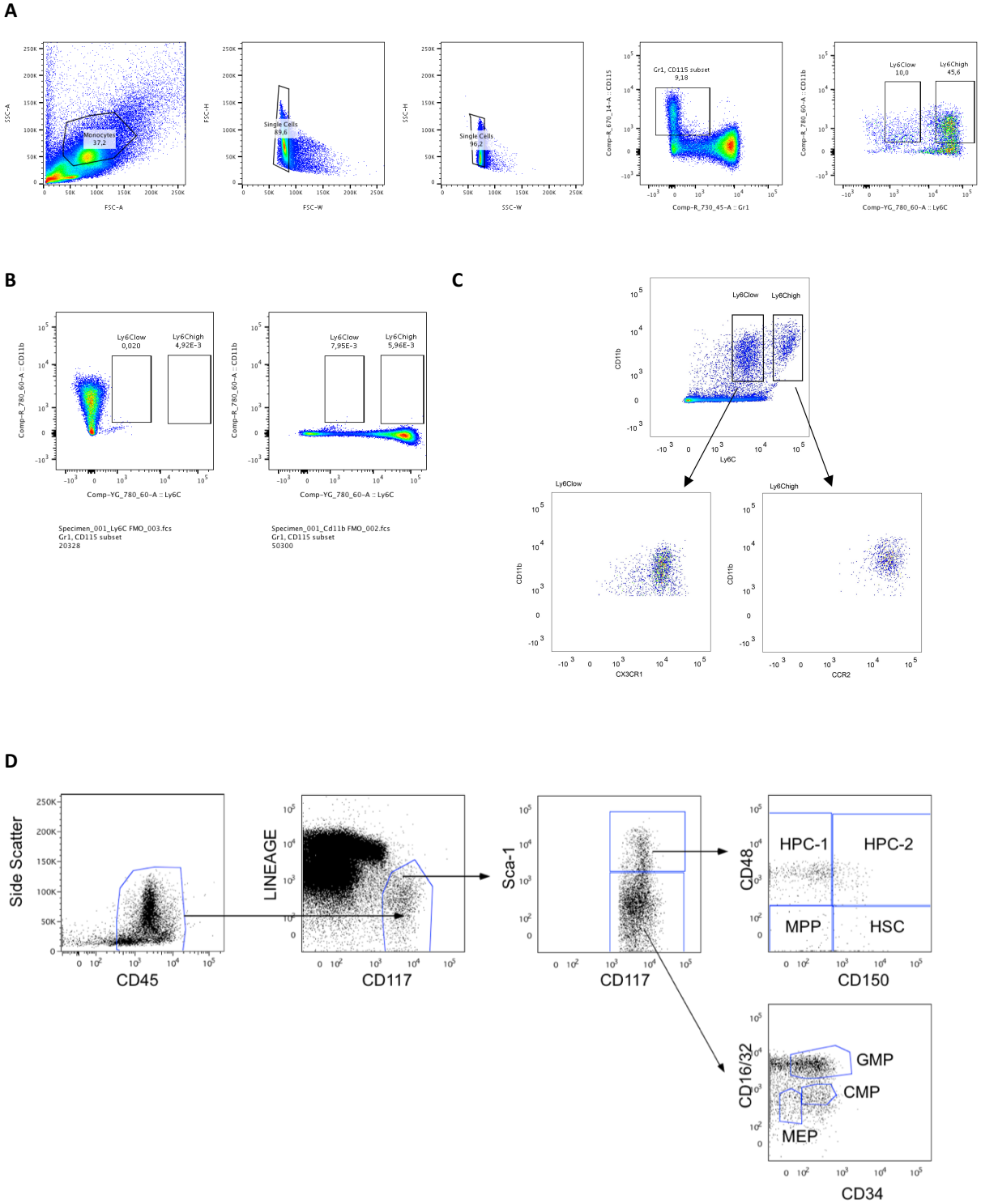

905

906 **Figure S4: Flow cytometry gating strategy for identification of Ly6C^{low} and Ly6C^{high} monocytes and**

907 **their precursor cells.** [A] Using side and forward scatter to identify singlet cells, CD115+Gr1- cells were

908 identified that were further analyzed using CD11b and Ly6C. [B] Ly6C^{low} and Ly6C^{high} monocyte gates
909 were drawn using fluorescence minus one (FMO) controls for CD11b and Ly6C. [C] The subsets were
910 further confirmed via CX3CR1 and CCR2, respectively. [D] CD45+ cells were analyzed using a lineage
911 cocktail (table 1) and CD117+, further broken down into Sca+ and – cells. Sca+ cells were further classified
912 using CD48 and CD150 while Sca- cells were further characterized via CD16/32 and CD34. Graph in panels
913 C was created using FlowJo software (Becton, Dickinson Company).

914

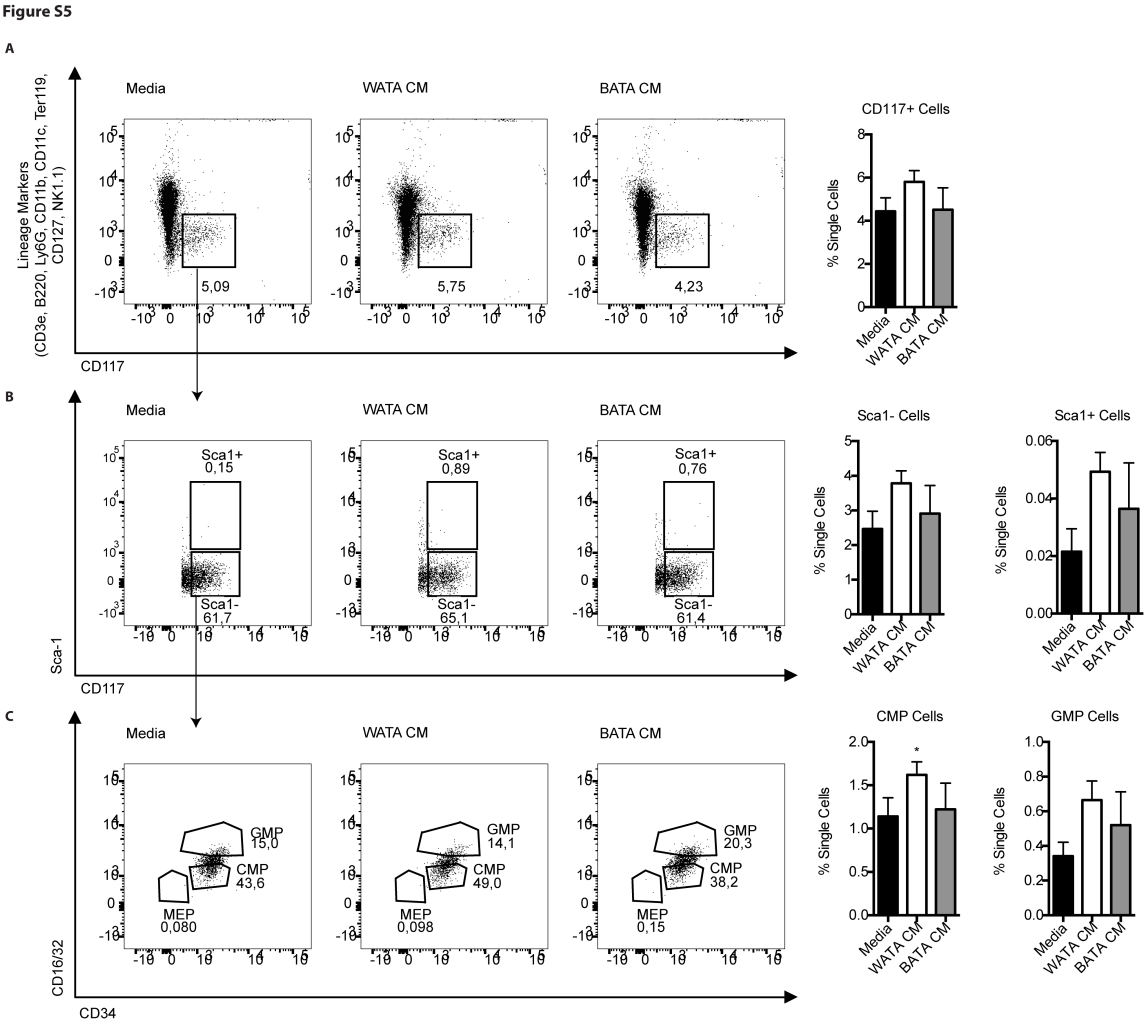

Figure S5: HSC and their progenitors using the panel of markers listed in table 1 following the white and brown CM treatment for 18 hours. [A-C] Flow cytometry analysis was used to test for the presence and changes in HSC and monocyte precursor cells in cultured monocytes treated with media, WATA-CM, and BATA-CM. Flow cytometry antibodies used are listed in Table 1. One way ANOVA test was used for statistical analysis. *P < 0.05.

921 **Table 1. List of Antibodies used for flow cytometry analysis.**

Markers	Fluorophore	Manufacturer	Clone	Catalog Number
CD11b	APC-eFluor 780	eBioscience	M1/70	47-0112-82
Ly6C	PE-Cy7	Biolegend	HK1.4	128018
Gr-1	Alexa Fluor 700	eBioscience	RB6-8C5	56-5931-82
CX3CR1	Brilliant Violet 421	Biolegend	SA011F11	149023
CCR2	Alexa594	R&D Systems	475301	FAB5538T
CD115	APC	eBioscience	AFS98	17-1152-82
F4/80	PerCP-Cy5.5	BioLegend	BM8	123128
CD11c	FITC	eBioscience	N418	11-0114-81
CD34	FITC	BD Biosciences	RA1434	553733
CD16/32	APC-R700	BD Biosciences	2.4G2	565502
CD45.2	BV650	BD Biosciences	30-F11	563410
CD150	PEPCP710	invitrogen	mShad150	46-1502-82
CD117	APC/Fire 750	BioLegend	2B8	105838
SCA1	PE-Cy7	invitrogen	D7	25-5981-82
CD48	BV605	BioLegend	MM48-1	103441
CD3e*	PE	BD Biosciences	17A2	555725
B220*	PE	BD Biosciences	RA3-6B2	553089
Ly6G*	PE	BD Biosciences	1A8	551461
CD11b*	PE	BD Biosciences	M1/70	553311
CD11c*	PE	BioLegend	N418	117308
Ter119*	PE	BD Biosciences	TER-119	553623
CD127*	PE	eBioscience	A7R34	12-1271-82
NK1.1*	PE	BD Biosciences	PK138	553165

922 *LINEAGE is a cocktail of antibodies containing CD3e, B220, Ly6G, CD11b, CD11c, Ter119, CD127,
923 NK1.1 with the same fluorophore to exclude all terminally differentiated cells.